MAX-DOAS O_4 measurements: A new technique to derive information on atmospheric aerosols—Principles and information content

T. Wagner, B. Dix, C. v. Friedeburg, U. Frieß, S. Sanghavi, R. Sinreich, and U. Platt

Institut für Umweltphysik, University of Heidelberg, Heidelberg, Germany

[1] Multi AXis Differential Optical Absorption Spectroscopy (MAX-DOAS) observations of the oxygen dimer O_4 which can serve as a new method for the determination of atmospheric aerosol properties are presented. Like established methods, e.g., Sun radiometer and LIDAR measurements, MAX-DOAS O_4 observations determine optical properties of aerosol under atmospheric conditions (not dried). However, the novel technique has two major advantages: It utilizes differential O_4 absorption structures and thus does not require absolute radiometric calibration. In addition, O_4 observations using this method provide a new kind of information: since the atmospheric O_4 profile depends strongly on altitude, they can yield information on the atmospheric light path distribution and in particular on the atmospheric aerosol profile. From O_4 observations during clear days and from atmospheric radiative transfer modeling, we conclude that our new method is especially sensitive to the aerosol extinction close to the ground. In addition, O_4 observations using this method yield information on the penetration depth of the incident direct solar radiation. O_4 observations at different azimuth angles can also provide information on the aerosol scattering phase function. We found that MAX-DOAS O_4 observations are a very sensitive method: even aerosol extinction below 0.001 could be detected. In addition to the O_4 absorptions we also investigated the magnitude of the Ring effect and the (relative) intensity. Both quantities yield valuable further information on atmospheric aerosols. From the simultaneous analysis of the observed O_4 absorption and the measured intensity, in particular, information on the absorbing properties of the aerosols might be derived. The aerosol information derived from MAX-DOAS observations can be used for the quantitative analysis of various trace gases also analyzed from the measured spectra.   *INDEX TERMS:* 0305 Atmospheric Composition and Structure: Aerosols and particles (0345, 4801); 0320 Atmospheric Composition and Structure: Cloud physics and chemistry; 0345 Atmospheric Composition and Structure: Pollution—urban and regional (0305); 0360 Atmospheric Composition and Structure: Transmission and scattering of radiation; *KEYWORDS:* atmospheric aerosol, MAX-DOAS

1. Introduction

[2] Atmospheric aerosols are important for various aspects of atmospheric chemistry and physics, they have in particular strong effects on the atmospheric radiation budget. Thus, human induced changes of the atmospheric aerosol load and its composition significantly contributes to climate change and affects human health. The lack of detailed knowledge on the optical properties of aerosols causes one of the largest uncertainties in climate forcing assessments [*Charlson et al.*, 1992; *Tegen and Lacis*, 1996; *Hansen et al.*, 1997; *Houghton et al.*, 2001].

[3] The influence of aerosols on the Earth's radiation budget and on atmospheric chemistry is complex, especially depending on the composition, size distribution, and shape of the aerosol particles [*Houghton et al.*, 2001; *Kaufman et al.*, 2002, 2003]. Apart from their direct effects on the solar and terrestrial radiation, aerosols also indirectly influence the Earth's radiation budget [*Feingold et al.*, 1999]. For example, high concentrations of fine aerosols can reduce the size of cloud droplets, increase their reflectance [*Twomey et al.*, 1984] and reduce precipitation [*Rosenfeld*, 2000; *Ramanathan et al.*, 2001; *Rosenfeld et al.*, 2002].

[4] Because of the strength and the complexity of the aerosol influence on the atmosphere, it is of special importance to improve our knowledge on these aerosol properties on a global scale [*Kaufman et al.*, 2002].

[5] In situ instruments like optical particle counters provide only data at the instrument location, moreover, usually only dry aerosol properties are determined. In addition, remote sensing methods have been developed for the measurement of aerosols, in particular Sun photometers and light detection and ranging (LIDAR) instruments.

[6] Sun photometer observations are performed since the late 1950s [*Volz*, 1959]. Usually the intensity (at different narrow wavelength intervals) of the direct solar radiation and the radiation scattered in the aureole region is measured [*Twitty*, 1975; *King et al.*, 1978; *Shaw*, 1979; *Box and Deepak*, 1979; *O'Neill and Miller*, 1984; *Tanré et al.*, 1988]. Additional measurement modes include observations over a larger angular range and observations of the state of polarization [*Nakajima et al.*, 1983; *Kaufman et al.*, 1994; *Vermeulen et al.*, 2000]. Sun photometer observations yield very precise values for the total aerosol extinction; also, information on the scattering phase function can be derived. From these quantities, information on the aerosol size distribution, the single scattering albedo and the refractive index can be extracted [*Twitty*, 1975; *King et al.*, 1978; *Shaw*, 1979; *Wang and Gordon*, 1993; *Wendisch and von Hoyningen-Hüne*, 1994; *Nakajima et al.*, 1996; *Devaux et al.*, 1998; *Romanov et al.*, 1999]. Sun photometers can be maintained automatically with high accuracy; the aerosol robotic network (AERONET) currently consists of more than 200 stations [*Holben et al.*, 1998].

[7] One of the main disadvantages of Sun photometers is that they can only measure optical properties of the total atmospheric column. In addition, since they observe the absolute value of the solar radiation, the requirements on instrument calibration and stability are high.

[8] LIDAR instruments use artificial light sources. They measure the intensity of the backscattered light as a function of time. Thus, LIDAR instruments are especially well suited for the retrieval of altitude information of the scattering properties of aerosols [*Collis*, 1966; *Sandford*, 1967; *Barrett and Ben-Dov*, 1967]. In addition, from the degree of depolarization information on the sphericity of the scattering particles (and thus on their physical state) can be derived.

[9] LIDAR instruments are well suited to derive the spatial distribution of atmospheric aerosols and they can also measure at night (sometimes only at night). However, the determination of quantitative estimates of the aerosol extinction or scattering coefficients is complicated by two major problems: the uncertainty in the aerosol backscatter-to-extinction ratio and the LIDAR calibration [*Klett*, 1981; *Fernald*, 1984]. Several approaches have been suggested to overcome theses fundamental limitations. For LIDAR instruments using a single wavelength, observations at different viewing angles allow to derive estimates for the backscatter-to-extinction ratio [*Sandford*, 1967; *Hamilton*, 1969; *Fernald et al.*, 1972; *Spinhirne et al.*, 1980; *Young et al.*, 1993]. A similar, but more sophisticated approach is the separation of emitter and receiver using a bistatic LIDAR setup [*Reagan et al.*, 1977; *Kunz*, 1987; *Hughes and Paulson*, 1988]. Also the combination with simultaneous Sun photometer observations can force the LIDAR inversion to yield quantitative values for the extinction coefficients [*Voss et al.*, 2001].

[10] Another elegant method is to use so called Raman LIDAR instruments which measure not only the elastically scattered intensity but also the Raman scattered signal, to which aerosol scattering does not contribute. Thus it is possible to separate the scattering and attenuation properties of aerosols [*Ansmann et al.*, 1990, 1992; *Wandinger et al.*, 1995; *Ferrare et al.*, 1998]. Because of the weak Raman signal, reliable Raman LIDAR observations are restricted to nighttime.

[11] We conclude that both Sun photometers and LIDAR instruments have their advantages and shortcomings. Sun photometers measure at various wavelengths and are capable providing information on the aerosol size distribution, phase function and extinction. However, no profile information can be inferred and all retrieved quantities refer to the total atmospheric column. LIDAR instruments can yield information on the atmospheric aerosol distribution at high spatial resolution. However, to infer quantitative results additional information (especially on the backscatter to extinction coefficient) or more sophisticated methods have to be used. Because LIDAR observations operate at a limited number of wavelengths, only limited information on the aerosol size distribution can be derived.

[12] Here we present a new method to derive aerosol information from passive optical observations using the DOAS method [*Platt*, 1994]. We show that from this method even information on the aerosol profile can be retrieved. Spectra of scattered sunlight are recorded and from these spectra the integrated absorption of the oxygen dimer O$_4$ is retrieved. This method was already applied to zenith sky observations at various wavelengths [*Wagner et al.*, 2002]. Here we extend the method to Multi-Axis-DOAS (MAX-DOAS) observations [*Hönninger and Platt*, 2002; *Leser et al.*, 2003; *von Friedeburg et al.*, 2004; *Bobrowski et al.*, 2003; *van Roozendael et al.*, 2003; *Wittrock et al.*, 2003; *Hönninger et al.*, 2004; A. Heckel et al., manuscript in preparation, 2004], which observe scattered sunlight from a variety of viewing directions (see Figure 1). In some studies MAX-DOAS O$_4$ observations were already successfully used for the determination of aerosol properties. The aerosol information has then been used for the interpretation of the MAX-DOAS observations of further trace gases of interest like HCHO or NO$_2$ [*Wittrock et al.*, 2003; A. Heckel et al., manuscript in preparation, 2004]. In this study, we develop a systematic and comprehensive analysis of the potential of MAX-DOAS O$_4$ observations of aerosols.

[13] Analyzing the differential O$_4$ absorption from the measured spectra has several advantages compared to the aerosol remote sensing instruments described above:

[14] 1. Since the MAX-DOAS O$_4$ analysis is a differential method, no absolute calibration is needed. In particular, degradation effects do not significantly influence the observed differential absorptions.

[15] 2. The observed O$_4$ absorption allows to conclude on the atmospheric distribution of photon paths, since the atmospheric O$_4$ concentration profile is well known and nearly constant. According to their altitude distribution, aerosols change the atmospheric photon path distribution in a characteristic way. Thus from MAX-DOAS O$_4$ observations, information on the atmospheric aerosol profile can be derived.
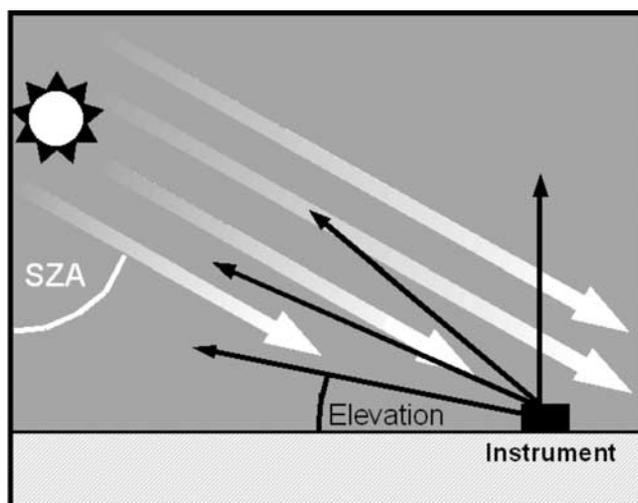
Figure 1. Scheme of the MAX-DOAS observation geometry. Scattered sunlight is observed under various elevation (and often also azimuth) angles. Often the elevation angle of the telescopes is defined with respect to the ground. The solar zenith angle (SZA) is defined as the angle between the incident sunlight and the zenith.

[16] 3. In addition to the O$_4$ absorption also the amount of Raman scattering can be retrieved from the MAX-DOAS spectra. Together with the O$_4$ absorption and the observed average (relative) intensity it might even be possible to separate the absorbing and scattering properties of aerosols.

[17] 4. O$_4$ absorption bands are distributed over the entire UV and visible wavelength range [*Greenblatt et al.*, 1990]. Thus it is possible to derive information on the wavelength dependence of various aerosol effects. The basic effects of aerosol scattering on several quantities derived from MAX-DOAS observations are summarized in Table 1.

[18] In this study we explore the potential of the proposed new method in three different ways. After a short introduction to the MAX-DOAS method, we first describe the basic effects of aerosol scattering on our observations. Second, we present examples of MAX-DOAS O$_4$ observations made on several clear days during the FORMAT II campaign in Milan/Italy in September 2003 (Formaldehyde as a tracer for oxidation in the troposphere (FORMAT) is a European research project, see: www.nilu.no/format/). During these days, the atmospheric aerosol load strongly increased. Third, we present and discuss results of numerical radiative transfer simu-

lations which confirm the findings of the two first sections. Finally, we summarize our results and show future potentials of the method.

2. MAX-DOAS Instrument and Data Analysis

[19] The MAX-DOAS instrument which was used during the FORMAT II campaign consists of three major components: a set of three moveable telescopes, which are connected via glass fiber bundles to a temperature stabilized imaging Czerny-Turner spectrograph with a two dimensional CCD-detector. The telescopes are directed at three different azimuth angles (5°, 185°, 250°) with respect to north. For simplicity we refer to these directions as north, south, and west, respectively. Each telescope sequentially scans 5 different elevation angles: 3°, 6°, 10°, 18° and 90° (zenith); a single measurement is taken every 90 seconds. The individual glass fibers from each bundle associated with the three different telescopes are arranged in a vertical column at the entrance slit of the spectrograph (with two gaps between the three fiber bundles, see Figure 2). The light is dispersed by a grating (1200 grooves per mm) and detected by a CCD array (1024 × 256 pixels over an area of 26.6 × 6,7 mm^2) with the wavelength axis in x-direction (from 320.4–457.2 nm) and the light from the different telescopes separated in y-direction (see Figure 2). Each spectrum from each of the individual telescopes covers about 55 lines on the CCD; these lines are added and yield the individual spectra for the different telescopes. The spectral resolution of our instrument is about 0.75 nm (FWHM). The gaps between the three spectra are about 40 lines wide (see Figure 2) and are used for a combined correction of electronic offset, dark current and spectrograph straylight for each individual measurement. This type of correction is especially important because of the largely varying amount of spectrograph straylight, which can reach up to about 20% in specific situations with large intensity differences between the different telescopes.

[20] The measured spectra are analyzed using the DOAS method [*Platt*, 1994]. To the (logarithm of the) measured spectrum several trace gas cross sections (see Table 2) as well as a Ring spectrum [*Grainger and Ring*, 1962; *Bussemer*, 1993], a Fraunhofer reference spectrum and a polynomial of degree 5 are fitted by means of a least squares fitting routine [*Gomer et al.*, 1993; *Stutz and Platt*, 1996]. As Fraunhofer spectrum, observations around noon in zenith direction were selected. Also included in the fitting routine was an inverse Fraunhofer spectrum (1/I$_0$) for the correction of a possibly remaining intensity offset. For the

Table 1. Overview on the Relationships Between Different Quantities Extracted From MAX-DOAS Observations and Aerosol Properties

Quantity Analyzed From MAX-DOAS Measurement	Derived Atmospheric Aerosol Properties
Modification of the O$_4$ absorption for different telescope elevations and SZA	⇒ total optical depth ⇒ information on the vertical profile
Wavelength dependence	⇒ size distribution
Azimuth dependence	⇒ phase function
Polarization dependence	⇒ phase function
Comparison of the measured intensity and O$_4$ absorption	⇒ single scattering albedo

Entrance slit

CCD-Array (256 lines by 1024 columns)

Telescope 1 (~55 CCD lines)

Gap (~40 CCD lines)

Telescope 2

Telescope 3

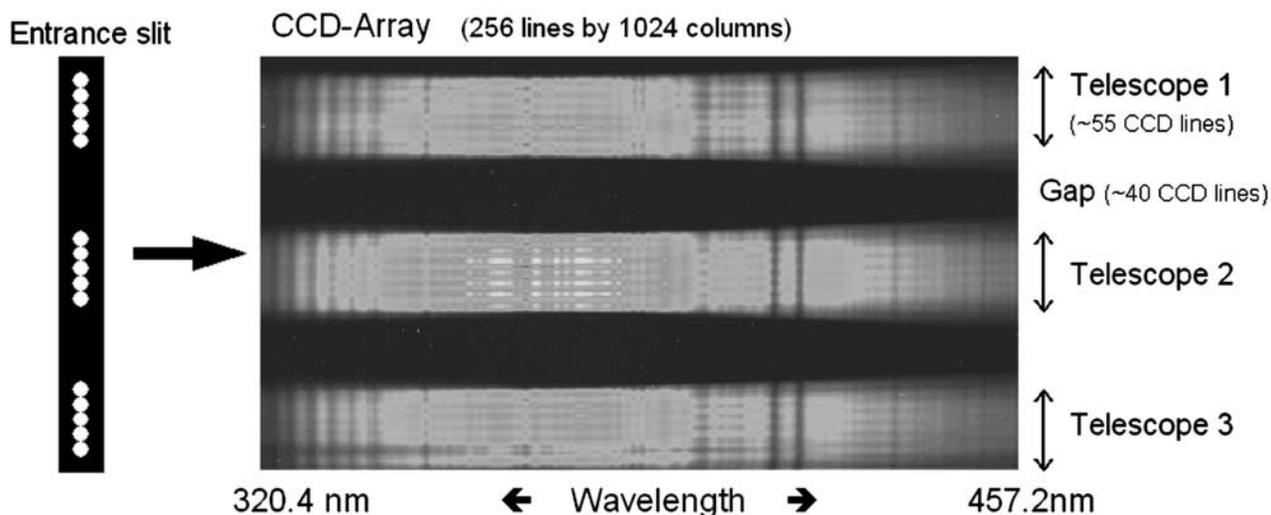320.4 nm ← Wavelength → 457.2nm

Figure 2. Projection of the three spectra on the two-dimensional CCD array. The three entrance slits (left) are formed by the exit ends of the fiber bundles. The gaps between the spectra are used for the correction of dark current, offset, and spectrograph stray light.

O_4 analysis the spectral range from $335-367$ nm was selected. The wavelength calibration was performed by fitting the measured spectra to a high resolution solar spectrum [*Kurucz et al.*, 1984]. An example of the DOAS O_4 analysis is shown in Figure 3.

[21] The result of the spectral analysis is the slant column density (SCD, the trace gas concentration along the absorption path). In the case of O_4, the SCD cannot be directly referred to O_4, because the equilibrium constant between O_4 and $(O_2)_2$ is not known. Therefore usually the O_4 SCD is referred to the integrated quadratic O_2 concentration [see also *Greenblatt et al.*, 1990]. The O_4 SCD then includes the equilibrium constant and it has the unit [$molec^2/cm^5$].

[22] Because the Fraunhofer spectrum also contains atmospheric absorption structures of O_4 (and other trace gases) the result of the DOAS analysis represents the difference of the SCDs of the measured spectrum and of the Fraunhofer spectrum; this difference is referred to as DSCD in the following. It should be noted that the Fraunhofer reference spectrum was selected in a way (telescope in zenith direction at small SZA during noon on September 14) that the O_4 SCD is small (about $2.2 \ 10^{43} molec^2/cm^5$, see section 5).

3. Influence of Aerosols on MAX-DOAS O₄ Measurements

[23] In contrast to direct light observations (using, e.g., the Sun or Moon as a light source), for scattered light observations the photons have traveled through the atmosphere on a variety of light paths. Thus for the detailed understanding and interpretation of scattered light observations usually radiative transfer models are applied [*Noxon et al.*, 1979; *Solomon et al.*, 1987; *Marquard et al.*, 2000]. For the interpretation of our MAX-DOAS observations (see section 5), we apply a Monte-Carlo radiative transport model [*von Friedeburg*, 2003; *Hönninger et al.*, 2004].

[24] In this section, our aim is to start with a discussion of the main characteristics of MAX-DOAS observations and the respective aerosol influence on these measurements in a simplified and more descriptive way. Figure 4 shows a simplified scheme of the atmospheric light paths relevant for MAX-DOAS observations for a given elevation angle. Also shown is the atmospheric height profile of the oxygen dimer O_4; due to its square dependence on the oxygen concentration its atmospheric scale height is only about 4 km.

[25] In order to illustrate the main effects of aerosols on the MAX-DOAS measurements, it is instructive to divide the total path of the scattered light into three segments (Figure 4): The first segment describes the incident sunlight penetrating into the atmosphere along a direct path. The penetration depth is determined by the optical depth with respect to Rayleigh and Mie scattering; in general, it is large for large wavelengths (because of the strong wavelength dependence of Rayleigh scattering, see Table 3), low aerosol load, and small solar zenith angle

Table 2. Trace Gas Cross Sections Used for the MAX-DOAS O₄ Analysis

Molecule	Data Source	Adaptation to Our Instrument
O₄ (296 K)	*Greenblatt et al.* [1990]	interpolation[a]
BrO (228 K)	*Wilmouth et al.* [1999]	convolution[b]
NO₂ (273 K)	*Vandaele et al.* [1997]	I₀-correction[c]
O₃ (221 K)	*Bogumil et al.* [2003]	I₀-correction[c]
O₃ (293 K)	*Bogumil et al.* [2003]	I₀-correction[c]
HCHO (298 K)	*Meller and Moortgat* [2000]	convolution[b]

[a]The cross section is interpolated to the wavelength grid of our instrument.

[b]The cross section is convoluted by the instrument function and interpolated to the wavelength grid of our instrument.

[c]The cross section is convoluted by the instrument function and interpolated to the wavelength grid of our instrument. In addition, a so-called I₀ correction is applied [*Aliwell et al.*, 2002].
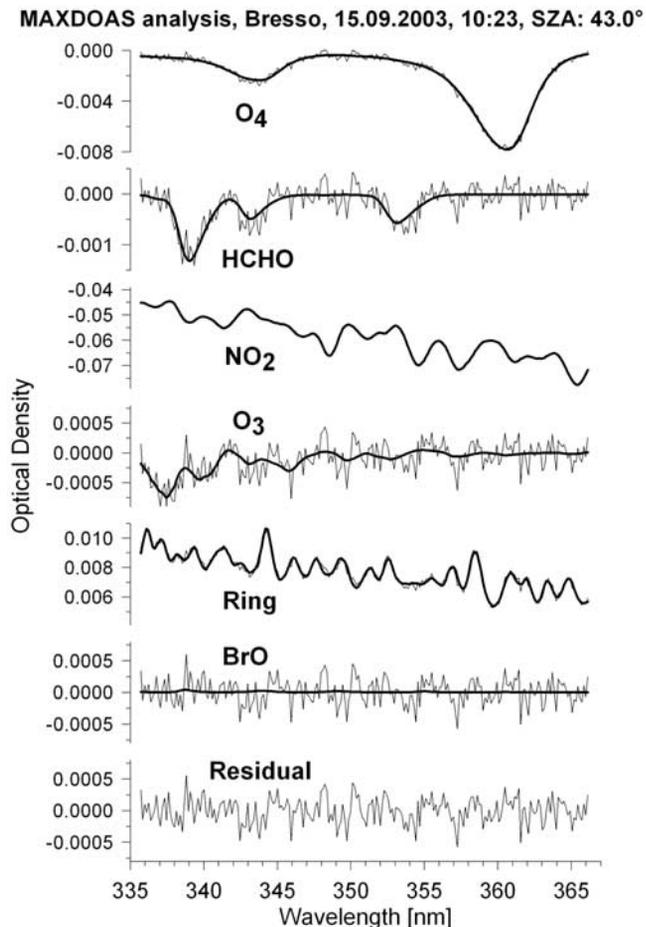
MAXDOAS analysis, Bresso, 15.09.2003, 10:23, SZA: 43.0°

Figure 3. Example of a spectral DOAS analysis. The thick lines show the trace gas cross sections scaled to the respective absorptions detected in the measured spectrum (thin lines). The mainly stratospheric trace gases O$_3$ and BrO show only a very weak absorption, because both the measured spectrum and the Fraunhofer reference spectrum contain nearly the same stratospheric absorption. In contrast, the trace gases with enhanced tropospheric concentrations show a large absorption (difference) since the measurement was taken at 3° elevation whereas the Fraunhofer reference spectrum was measured in zenith direction (see section 3).

(SZA). After this first segment, the photons might enter a multiple scattering layer (Figure 4, bottom). Especially inside thick clouds, multiple Mie-scattering can cause extended layers of diffuse radiation in which the photons have lost their 'memory' of direction [*Erle et al.*, 1995; *Wagner et al.*, 1998; *Veitel et al.*, 1998; *Pfeilsticker*, 1999; *Pfeilsticker et al.*, 1998, 1999]. However, for many measurement situations (especially for clean air and/or for large wavelengths) the optical depth of the atmosphere is rather small and no significant multiple scattering layer establishes. Finally the photons are scattered into the field of view of the telescopes of the instrument. Similarly to the penetration depth of the incident sunlight also the length of the direct light paths along the line of sight of the telescopes depends on the optical depth with respect to Rayleigh and Mie scattering; short direct light paths occur especially for small wavelengths and high aerosol load. It is interesting to note that the length of the direct light path along the line of sight of the telescopes (especially for low elevation angles) is directly related to the visibility of the atmosphere close to the ground (see, e.g., Table 4).

[26] Owing to their scattering and absorbing properties, aerosols modify all of the three described segments of the atmospheric light path compared to a pure Rayleigh atmosphere. The most important effects of aerosols are as follows (see Figure 4, bottom):

[27] 1. Reduction of the visibility: Aerosols reduce the visibility of the atmosphere and thus decrease the direct light paths of the incident solar radiation and along the line of sight of the telescopes. These effects will, in general, reduce the observed O$_4$ absorptions.

[28] 2. Increased probability of multiple scattering: Aerosols increase the number of scattering events, especially in the case of extended clouds. This effect will in general lead to a simultaneous increase of the O$_4$ absorption for all viewing angles [*Erle et al.*, 1995; *Wagner et al.*, 1998, 2002].

[29] 3. Modification of the received intensity: Aerosol scattering increases the total amount of scattered photons and thus, in general, enhances the observed intensity. For high aerosol concentrations (especially also for thick clouds) this effect, however, can be (over-) compensated by aerosol extinction along the line of sight. Especially for absorbing aerosols the light intensity is further reduced. In contrast to Rayleigh scattering, aerosol scattering usually strongly prefers the forward direction. Thus the effect of aerosol scattering is significantly different for telescopes looking at different elevations and, especially, different azimuth angles.

[30] These modifications of the atmospheric light paths change the relative composition of light paths having experienced different atmospheric O$_4$ absorptions and thus make MAX-DOAS O$_4$ measurements especially sensitive to the influence of aerosols. Since the atmospheric O$_4$ profile is located close to the surface (the scale height is about 4 km), aerosol scattering at different altitudes has different effects on the observed O$_4$ absorption. This makes MAX-DOAS O$_4$ absorptions (in contrast to measurements of the absolute intensity) particularly sensitive to the atmospheric altitude distribution of aerosols. As will be shown in section 5 the aerosol absorption has a significantly different influence on the observed O$_4$ absorption compared to the measurements of the absolute intensity. Therefore, from the simultaneous analysis of the O$_4$ absorption and the measured light intensity, also conclusions on the absorbing properties of aerosols might be drawn.

[31] Since aerosol scattering also changes the relative contribution of elastic scattering (due to molecules and aerosols) and inelastic molecular scattering events, it also modifies the strength of the Ring effect (the filling-in of Fraunhofer lines [see *Grainger and Ring*, 1962; *Kattawar et al.*, 1981; *Bussemer*, 1993]), which can also easily be derived from MAX-DOAS observations.

[32] In sections 4 and 5, we present measurements and radiative transfer modeling results, which in detail investi-
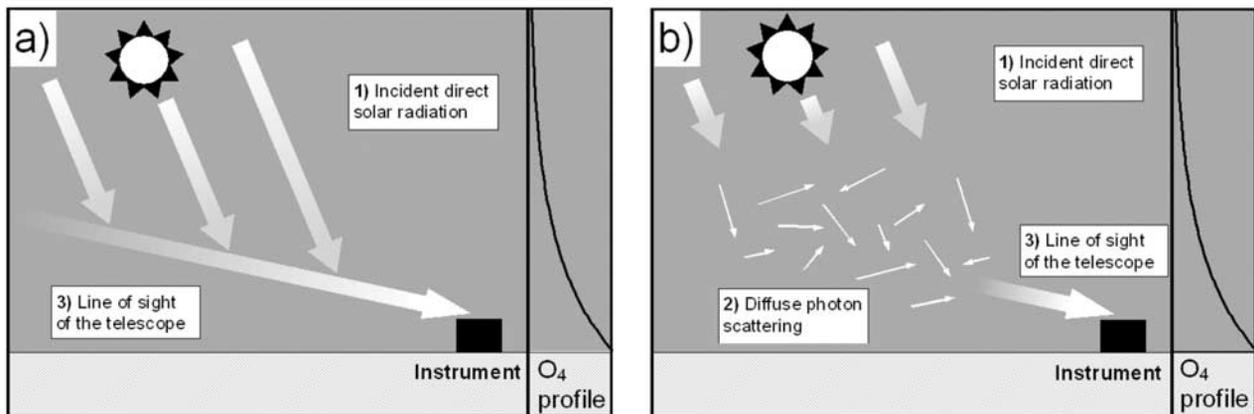
Figure 4. (a) Scheme of the different segments of the atmospheric light paths for MAX-DOAS observations. For an optically thin atmosphere, e.g., for an atmosphere without aerosol scattering and observations in the visible spectral range the observed photons are mainly single scattered. The penetration depth of the direct sunlight is large (first segment); also the direct line of sight of the telescopes (third segment) is long. (b) If additional aerosol scattering takes place, the direct line of sight of the telescopes decreases. Since the majority of the atmospheric O$_4$ is located close to the ground, the observed O$_4$ absorption is then also significantly decreased. Additional aerosol scattering also decreases the penetration depth of the incident direct solar radiation. For very strong aerosol scattering (e.g., inside extended clouds) also a regime of diffuse multiple photon scattering can occur which can enhance the O$_4$ absorption.

gate these effects of aerosols on MAX-DOAS observations of the O$_4$ absorption, on the (relative) light intensity, and the Ring effect.

4. MAX-DOAS Observations During a Period of Increasing Aerosol Load

[33] For the analysis of MAX-DOAS O$_4$ observations, we focus on a measurement period of four mostly clear days during the FORMAT II campaign in Milan, Italy in September 2003 (see http://www.nilu.no/format/). During these days the aerosol load of the atmosphere was strongly increasing. At the beginning, on September 14, the atmosphere was very clear after a series of rainy days. The atmospheric visibility was very high and even the Monte Rosa mountain at a distance of about 120 km was clearly visible. During the following days the atmospheric visibility was steadily decreasing. Finally, even the southern edge of the Alpine mountains at a distance of only about 30 km was not visible anymore.

[34] In Figure 5 the respective MAX-DOAS O$_4$ observations for the southern telescopes are presented. Except for the morning of September 15, the diurnal variation of the O$_4$ absorptions is smooth and almost symmetric, indicating that

the sky was clear throughout most of the period. Nevertheless, the magnitude of the O$_4$ absorption and also the amplitude of the diurnal variation of the O$_4$ absorptions change significantly during the following days, which can be attributed to the influence of additional aerosol scattering. Different aerosol effects can be distinguished, which are described in the sections below.

4.1. Reduction of the Direct Light Path Along the Line of Sight

[35] Aerosol extinction reduces the direct light path along the line of sight of the telescopes (see Figure 4). The higher the aerosol load is, the shorter is the distance from which photons can reach the telescopes on a direct path. Thus especially the O$_4$ absorptions for telescopes with low elevation angles are strongly reduced for high aerosol extinction. This aerosol effect can clearly be identified in our O$_4$ observations (Figure 5). In particular, interesting is also the fact that the differences of the O$_4$ absorptions for all low elevation telescopes (3°, 6°, 10°, 18°) significantly decrease during the period. This indicates that due to additional aerosol scattering the direct light paths along the line of sight become nearly independent on the elevation angle.

Table 3. Optical Depth of the Atmosphere as a Function of Wavelength and Telescope Elevation Angle (With Respect to Rayleigh Scattering)[a]

Elevation Angle, deg	Wavelength, nm		
	350	450	700
3	10.95	4.01	0.68
10	3.30	1.21	0.21
90	0.57	0.21	0.04

[a]For an optically thin (thick) atmosphere the probability of a photon to be multiple scattered is low (high).

Table 4. Properties of the Aerosol Profiles Used for the Radiative Transfer Simulations

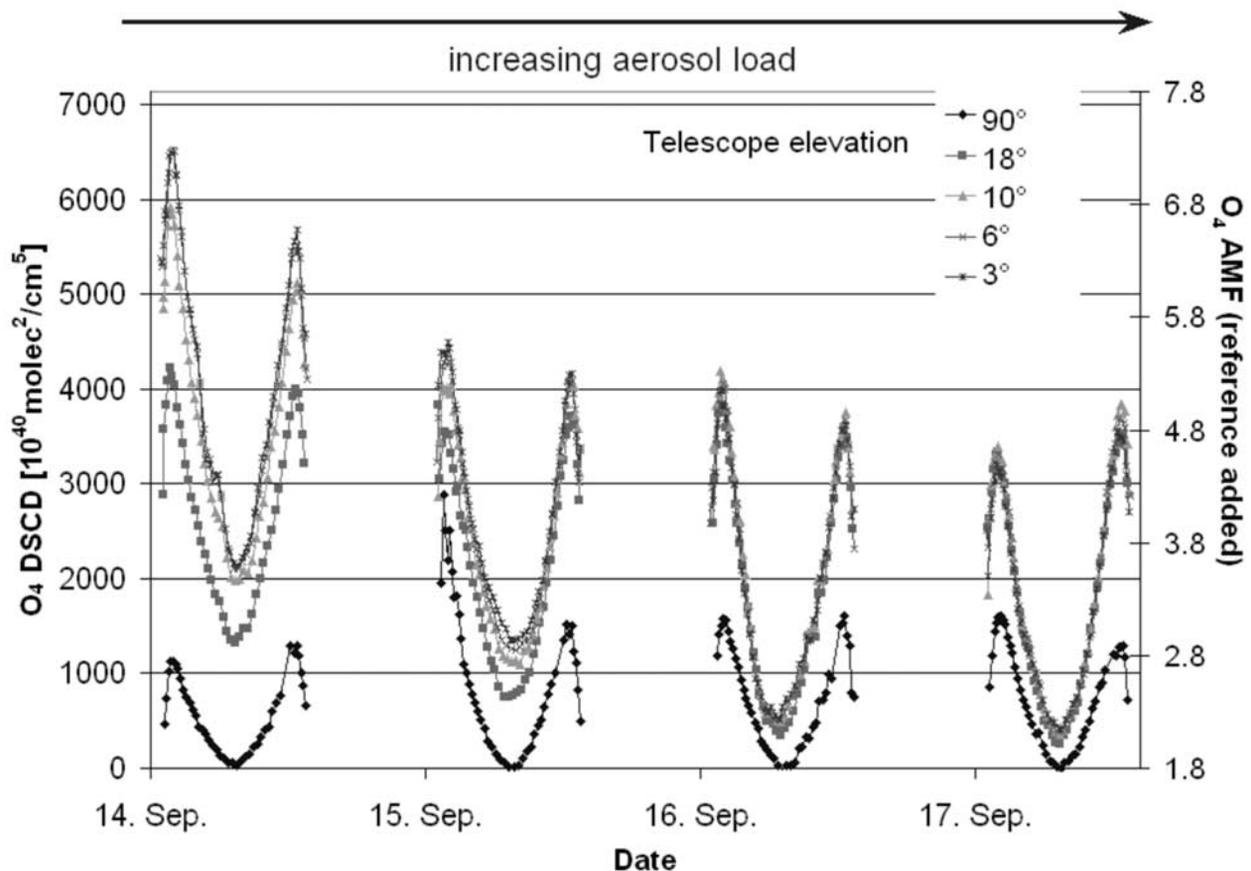| Profile Name	Aerosol Extinction	Altitude Range, km	Total Aerosol Extinction	Visibility, km (Mie Only)
0.05_2	0.05/km	0–2	0.1	78
0.1_1	0.1/km	0–1	0.1	39
0.1_2	0.1/km	0–2	0.2	39
0.5_1	0.5/km	0–1	0.5	8

Figure 5. O_4 DSCDs measured for different elevation angles of the southern telescope during four mostly clear days (September 14–17, 2003) at Milan, Italy. Because of the changing Sun position during the day the relative azimuth angles of the telescopes with respect to the Sun are ~90° during sunrise, ~0° during noon, and ~−90° during sunset. The main effects are the general reduction of the observed O_4 absorption and the decreasing difference between the low elevation telescopes (3°, 6°, 10°, 18°). These effects can be related to the increased aerosol load during the selected period (see text). The zenith observations during the morning of September 15 were affected by sporadic clouds and should not be taken into account for the detailed interpretation of the time series. With the knowledge of the O_4 VCD and the O_4 absorption of the Fraunhofer reference spectrum, the measured O_4 DSCD can also be expressed as (absolute) air mass factor (AMF, see section 5). For the comparison of the measurements to radiative transfer models the respective AMF is also shown (right axis). See color version of this figure at back of this issue.

[36] A simple way to quantify this decrease is to compare the observations around noon, when the atmospheric light path of the incident sunlight is smallest. For this time of the day, the difference between the 3° telescope and the zenith telescope decreases by a factor of 5 (from about $2.1 \cdot 10^{43}$ molec²/cm⁵ to $0.4 \cdot 10^{43}$ molec²/cm⁵) from September 14 to 17.

4.2. Influence on the Penetration Depth of the Incident Sunlight

[37] Aerosol scattering changes the penetration depth of the incident sunlight and thus the amplitude of the diurnal variation of the measured O_4 absorption. Two different situations have to be considered:

[38] For an optically thin atmosphere (e.g., for zenith viewing telescopes and/or for measurements at long wavelengths, see Table 3) a large fraction of the incident photons traverses the atmosphere without being scattered into the instrument. In the case of additional aerosol scattering part of

these photons are also scattered into the instrument. Since the bulk of atmospheric aerosols is usually located close to the surface the average scattering altitude of the measured photon is decreased compared to the pure Rayleigh case (for high clouds also an increase of the average scattering altitude can take place [*Wagner et al.*, 1998]). Accordingly, the effective penetration depth of the incident sunlight is increased and so is the amplitude of the diurnal variation of the O_4 absorption. In our measurements this effect can be identified for the zenith pointing telescopes: during the selected period the diurnal variation of the zenith telescope increases from about $1.1 \cdot 10^{43}$ molec²/cm⁵ to $1.6 \cdot 10^{43}$ molec²/cm⁵. The high values on the morning of September 15 should be ignored here because they can be related to sporadic clouds.

[39] For an optically thick atmosphere (see Table 3) the probability for an incident photon to be scattered is already close to unity. Now, the main effect of additional aerosol scattering is to reduce the penetration depth of the incident sunlight, because of the reduced visibility. The
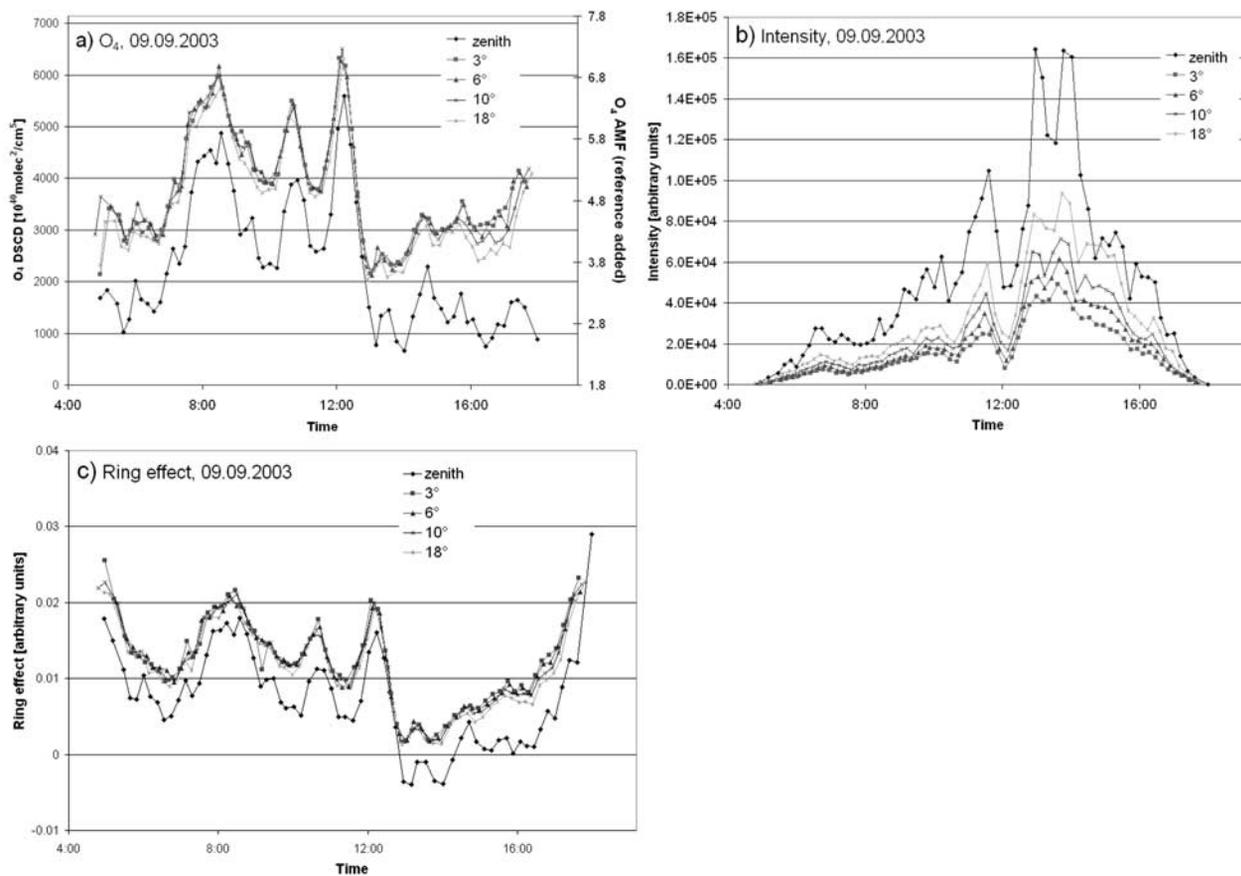
Figure 6. (a) O$_4$ DSCDs for a cloudy day (September 9) during the FORMAT II campaign (for the AMF-scale, see Figure 5). During the whole day the sky was overcast. The synchronous diurnal variation of the O$_4$ absorption for all telescopes indicates that the absorption path for O$_4$ is dominated by multiple scattering inside the clouds. The nearly constant difference between the low elevation angles (3°, 6°, 10°, 18°) and the zenith direction can be referred to different light paths below the cloud layer. (b) Relative intensities for September 9. Around 12:00 the appearance of a thick cloud is indicated by a reduced intensity for all telescopes. (c) Ring effect for September 9. Around 12:00 the Ring effect (and the O$_4$ absorptions) for all telescopes are simultaneously enhanced.

corresponding reduction of the diurnal variation can be especially expected for the telescopes at low elevation angles (see Figure 4). In our MAX-DOAS O$_4$ observations, this effect can be identified for the low elevation telescopes (Figure 5). On the first day, the amplitude of the diurnal variation ranges from $2.8 \cdot 10^{43}$ molec^2/cm^5 for the telescope with 18° elevation to $4.5 \cdot 10^{43}$ molec^2/cm^5 for the telescope with 3° elevation. During the following days these amplitudes decrease to about only $2.8 \cdot 10^{43}$ molec^2/cm^5 for all low elevation telescopes.

[40] It is interesting to note that the amplitude of the diurnal variation is sensitive not only to the aerosol extinction but also to the height of the aerosol layer (see also section 5). Thus from the diurnal variation also information on the vertical profile of the aerosol concentration could be derived. An indication of this possibility can be seen at the last two days of the selected period. For these days the diurnal variation changes (from about $3.5 \cdot 10^{43}$ molec^2/cm^5 to $2.8 \cdot 10^{43}$ molec^2/cm^5), although the O$_4$ absorption of the low elevation telescopes during noon is similar (about $0.4 \cdot 10^{43}$ molec^2/cm^5). This finding is a hint that the vertical extent of the aerosol layer has increased from September 16

to 17, leading to a reduced penetration depth of the incident sunlight.

4.3. Effect of Multiple Scattering

[41] At low aerosol levels (and in particular at relatively long wavelengths) the bulk of the light recorded by the spectrometer is only scattered once [e.g., *Perliski and Solomon*, 1993]. However, for high aerosol concentrations, a layer can occur in which the photons undergo diffuse multiple scattering (see Figure 4). In such cases, a (nearly constant) additional O$_4$ absorption is added to the measurements for all viewing directions. During the selected period of clear days (Figure 5) we found no indication for such a multiple scattering regime. However, a simultaneous increase of the O$_4$ absorption for different elevation angles can be often observed for vertically extended clouds, e.g., on September 9 (Figure 6) [see also *Erle et al.*, 1995; *Wagner et al.*, 1998, 2002].

4.4. Influence of Aerosol Absorption

[42] The distribution of the atmospheric light paths which contribute to the observed light is largely determined by
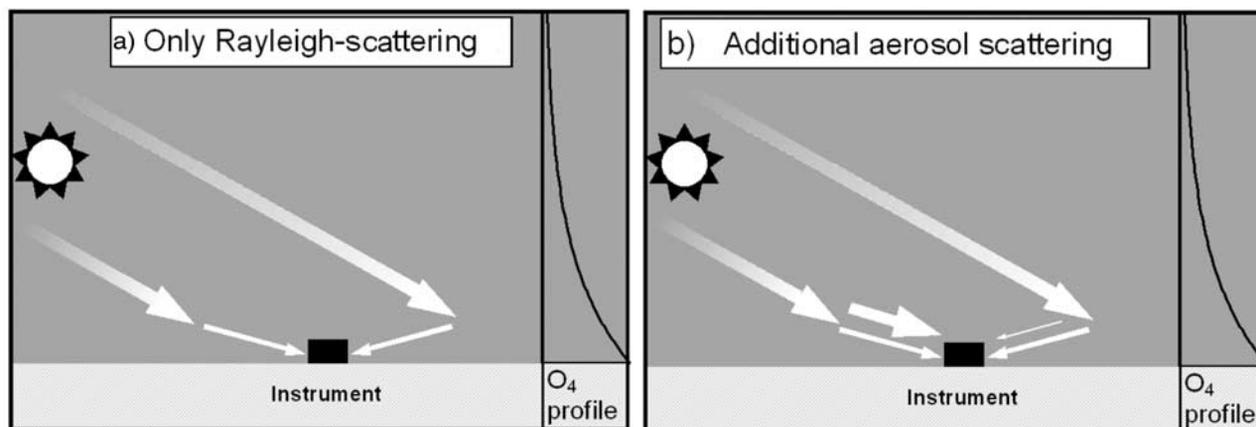
Figure 7. (a) For a pure Rayleigh atmosphere a telescope directed toward the Sun and another away from the Sun receives nearly the same amount of photons. (b) Influence of aerosol scattering for observations at similar (small) elevation angles but different azimuth angles (0° and 180° with respect to the Sun). Additional aerosol scattering strongly prefers the forward direction, and the telescope directed toward the Sun receives more single scattered photons compared to the telescope directed away from the Sun.

aerosol and molecular scattering. Thus the aerosol induced deviation of the O$_4$ absorption from the Rayleigh case is primarily an indicator of the scattering properties of aerosols and is, in general, only weakly affected by aerosol absorption. Additional aerosol absorption, however, decreases the absolute values of the observed intensity. Since this reduction affects both the center and the wings of the O$_4$ absorption bands the differential optical depth of the O$_4$ absorption is only slightly affected (see also section 5). Information on the absorbing properties of aerosols might thus be retrieved if both the measured O$_4$ absorption and the broadband intensity are taken into account for the interpretation of the MAX-DOAS observation. For a given O$_4$ absorption, a reduced intensity indicates a stronger aerosol absorption. This effect is not clearly obvious in our observations but an indication might be seen on September 16 and 17. While during noon the O$_4$ absorption is nearly similar for the low elevation telescopes (Figure 5), the observed intensity is significantly lower on September 17 (intensity of the southern telescopes, see Figure 10, center and bottom) possibly because of elevated aerosol absorption on that day. However, it should be noted that, so far, the experimental evidence on the retrieval of the absorbing properties is neither clear nor comprehensive and has to be confirmed in future studies.

4.5. Influence of the Scattering Phase Function

[43] The angular dependence of aerosol scattering differs significantly from that of molecular scattering. In particular, aerosol scattering strongly prefers the forward direction. Thus the influence of aerosols on the observed O$_4$ absorption is different for different azimuth angles (at moderate to large SZA). Assuming, e.g., a solar zenith angle of 40° and two telescopes at 3° elevation, one directed toward the Sun and the other away from the Sun (Figure 7), the probability for Rayleigh scattering is almost similar for both telescopes and the same O$_4$ absorptions (and light intensities) should be measured for an atmosphere without aerosols. In contrast, if aero-

sols are present, forward scattering of the incident sunlight becomes much more pronounced, and the telescope directed toward the Sun receives more single scattered photons than the other telescope. In the considered case (SZA = 40°), the O$_4$ absorptions of single scattered photons are on average smaller than those of multiple scattered photons, since the latter have traveled a longer path through the lower part of the atmosphere. Consequently, the O$_4$ absorption of the telescope directed toward the Sun becomes smaller than that of the other telescope. The magnitude of this difference depends on the frequency of aerosol scattering and on the scattering phase function.

[44] This azimuth effect can be clearly identified in our MAX-DOAS O$_4$ observations, especially for the low elevation angles of the northern and southern telescopes (Figure 8). The O$_4$ absorptions of the southern telescopes are smaller than those of the northern telescopes almost throughout the selected period, indicating a higher fraction of single scattered photons. Another interesting finding is that this difference becomes smaller toward the end of the period (especially for the lowest elevation angle of 3°). This is an indication that for an increasing aerosol load the influence of multiple scattering increases. In consequence, the relative contribution of the single scattered light becomes smaller and correspondingly also the differences of single scattered light for different azimuth angles are reduced.

[45] It is interesting to consider also the western telescope. Here we find that during the first half of the day (azimuth ~90°) the observed O$_4$ absorption is similar or even higher than for the northern telescope. This is in agreement with the expectation that for Rayleigh scattering the 90° scattering angles are strongly suppressed. During the afternoon, however, the observed O$_4$ absorptions fall below even those of the southern telescopes, because then the azimuth angle between the western telescope and the Sun is close to zero and the probability of aerosol scattering is high.
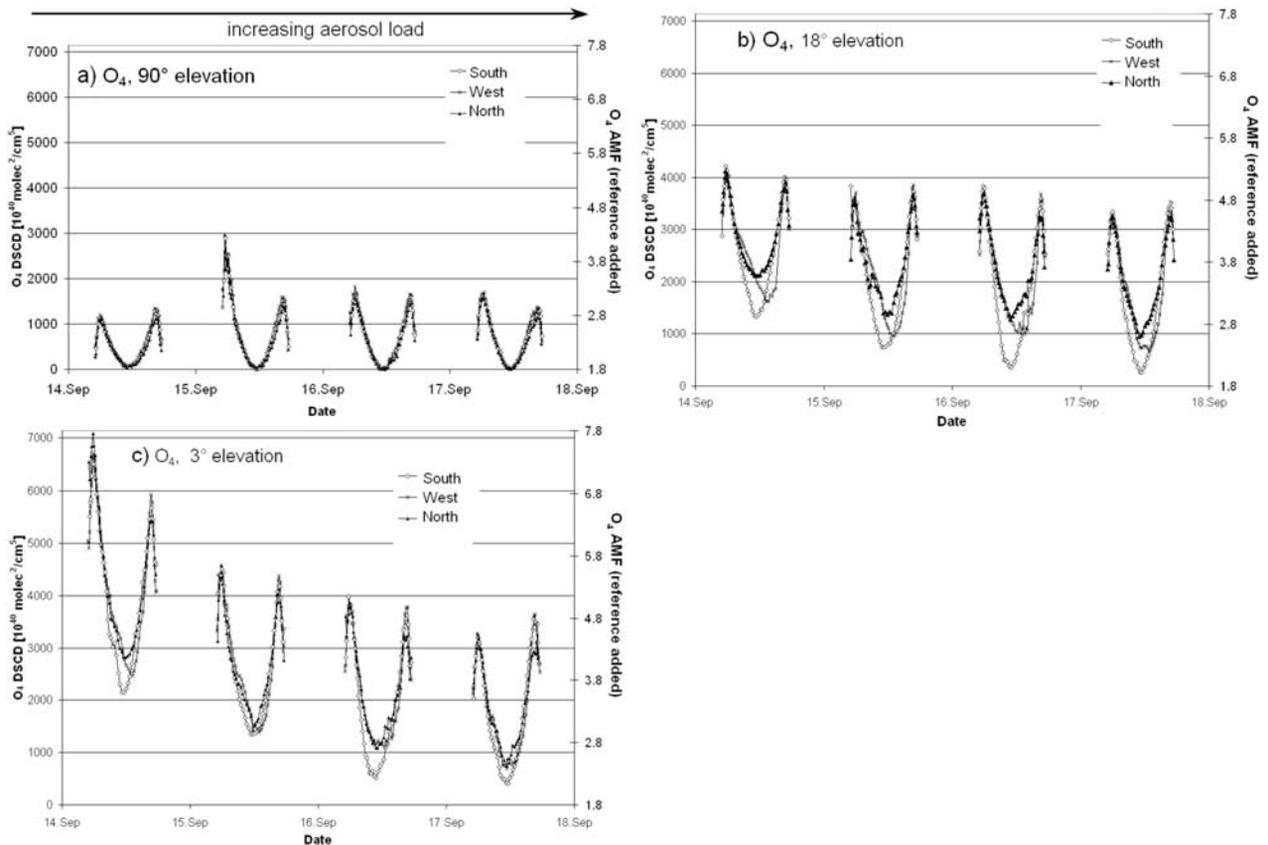
Figure 8. (a) Measured O$_4$ DSCDs for the different telescopes (north, south, west) at 90° elevation for September 14 to 17 (for the AMF-scale see Figure 5). The observations during the morning of September 15 were affected by clouds and should not be taken into account for the detailed interpretation of the time series. (b) Measured O$_4$ DSCDs for 18° telescope elevation and different azimuth angles (north, south, west). (c) Measured O$_4$ DSCDs for 3° telescope elevation and different azimuth angles (north, south, west).

[46] The above discussed effects of aerosols on MAX-DOAS O$_4$ absorptions are summarized in Figure 9. For the various MAX-DOAS geometries and solar zenith angles, aerosol scattering and absorption influence the O$_4$ absorption in a characteristic way. It should be noted that for reasons of clarity Figure 9 displays only a small subset of possible MAX-DOAS geometries; in addition, it is restricted to only one wavelength. At different wavelengths, the aerosol influence on MAX-DOAS O$_4$ absorptions can become significantly different (see, e.g., Figure 16).

4.6. Aerosol Influence on the Intensity of Scattered Radiation and on the Ring Effect

[47] Our interpretation of the influence of aerosols on the atmospheric light paths for different azimuth angles can be confirmed by considering further observed quantities. For that purpose we also investigated the observed average intensity between 335 and 366 nm (Figure 10) and the magnitude of the Raman-scattered light, the so-called Ring effect (Figure 11). From the measurement of the intensity we can clearly confirm the conclusions drawn from the O$_4$ absorptions in section 4.5. In Figure 10, it is obvious that the intensity of the northern telescope is always smaller than that of the southern

telescope. In addition, the intensity of the western telescope is smallest in the morning and highest in the afternoon. Both findings are in agreement with the difference of the O$_4$ absorptions for the different azimuth angles.

[48] We can also study the influence of the increasing aerosol load on the intensity during the four days. The behavior is different for the zenith and low elevation telescopes. For the zenith direction the intensities for September 15–17 are significantly enhanced compared to September 14 indicating that the telescopes receive additional photons due to aerosol scattering. For the 18° telescopes, the intensity first increases (September 15), but later gradually decreases because of increasing aerosol extinction along the line of sight. For the 3° telescopes the latter effect dominates throughout all days and the intensities decrease from September 14–17.

[49] The magnitude of the Ring effect (e.g., expressed as the strength of the filling-in of a Fraunhofer line [see, e.g., *Grainger and Ring*, 1962]) is a measure for the relative contribution of light having undergone rotational Raman scattering to the measured total intensity. Rotational Raman scattering occurs only for scattering on molecules; the probability of a photon being Raman scattered is about a few percent [*Bussemer*, 1993; *Chance and Spurr*, 1997].
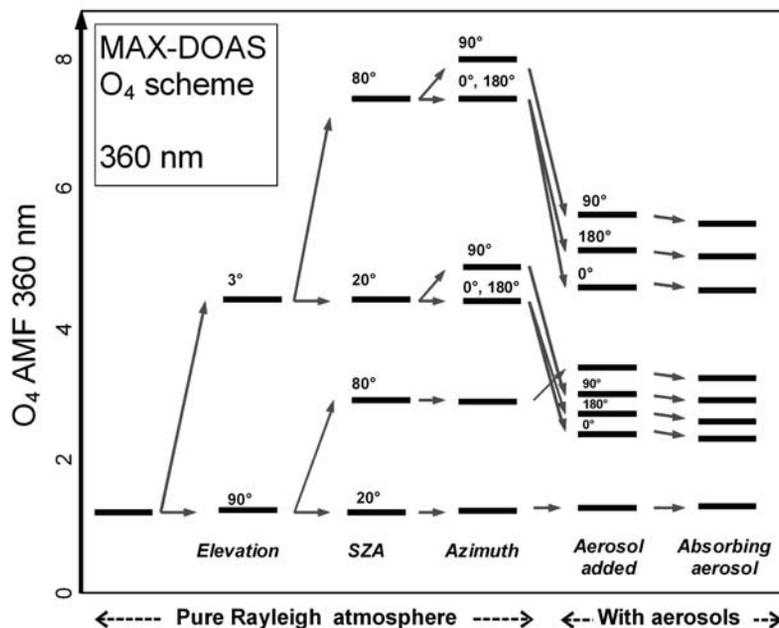
Figure 9. Overview on the influence of aerosols on MAX-DOAS O$_4$ observations for 360 nm (expressed as AMF, see section 5). Along the x-axis the possible MAX-DOAS geometries are shown (the first case is for a SZA of 20° and a telescope elevation of 90°). Even for a pure Rayleigh atmosphere a large variety of different O$_4$ absorptions is found. If aerosols are added, these O$_4$ observations are modified in a characteristic way depending on the aerosol properties (the aerosol extinction was set to 0.5/km, and the single scattering albedo was either set to 0 or 0.5). In contrast to the absolute intensity the influence of the aerosol single scattering albedo on the O$_4$ absorption is relatively weak. It should be noted that similar schemes for O$_4$ absorption bands at other wavelengths show different dependencies indicating additional information content of multiwavelength MAX-DOAS observations. Also the observation of the O$_4$ absorption for light with different polarization might add valuable further information.

The magnitude of the Ring effect thus depends on the specific conditions of a given measurement. Two different cases have to be considered:

[50] 1. The first case is measurements in which mainly single scattered photons are received by the telescope (e.g., zenith sky observations under clear sky at large wavelengths, see Table 3). In this case the relative contribution of Raman scattered photons decreases if additional (elastic) scattering on aerosols takes place. Consequently, the magnitude of the Ring effect decreases with increasing frequency of aerosol scattering.

[51] 2. The second case is measurements in which mainly multiple scattered photons are received by the telescope (especially observations under cloudy sky). In this case additional aerosol scattering increases also the probability of a photon to be scattered again by a molecule and thus to undergo additional Raman scattering. Consequently, now the magnitude of the Ring effect increases with increasing frequency of aerosol scattering. This effect can be clearly seen for measurements under extended clouds (Figure 6), when multiple Mie scattering takes place.

[52] As can be seen in Figure 11, the amount of the Ring effect is indeed a very sensitive indicator of the specific contributions of molecular and aerosol scattering. The Ring effect of the southern telescopes, e.g., is always systematically lower compared to that of the northern telescopes indicating that for the southern telescopes the fraction of

photons being single scattered at aerosols is higher because of the pronounced forward scattering of aerosols. Similar findings can be found for the western telescope where the Ring effect is strongest in the morning and smallest in the afternoon indicating that the fraction of photons being single scattered at aerosols is smallest during morning and highest during afternoon when the telescope is pointing almost to the Sun.

[53] During the whole four days the magnitude of the Ring effect decreases for all viewing directions (except for the 3° elevations on September 16 and 17). This reflects the fact that aerosol scattering increases the relative fraction of photons which have been scattered only elastically. It also indicates that despite the high concentration of aerosols most of the received photons are still only single scattered.

[54] From these findings we conclude that not only the O$_4$ absorption but also the measured broadband intensity and the Ring effect are influenced by aerosol scattering in a significant and characteristic way, and thus contain useful information on atmospheric aerosols properties.

5. Radiative Transport Modeling

[55] In this section we present results of radiative transfer modeling for MAX-DOAS O$_4$ observations at different atmospheric aerosol conditions. The simulations are carried out with the Monte Carlo model 'TRACY,' which takes
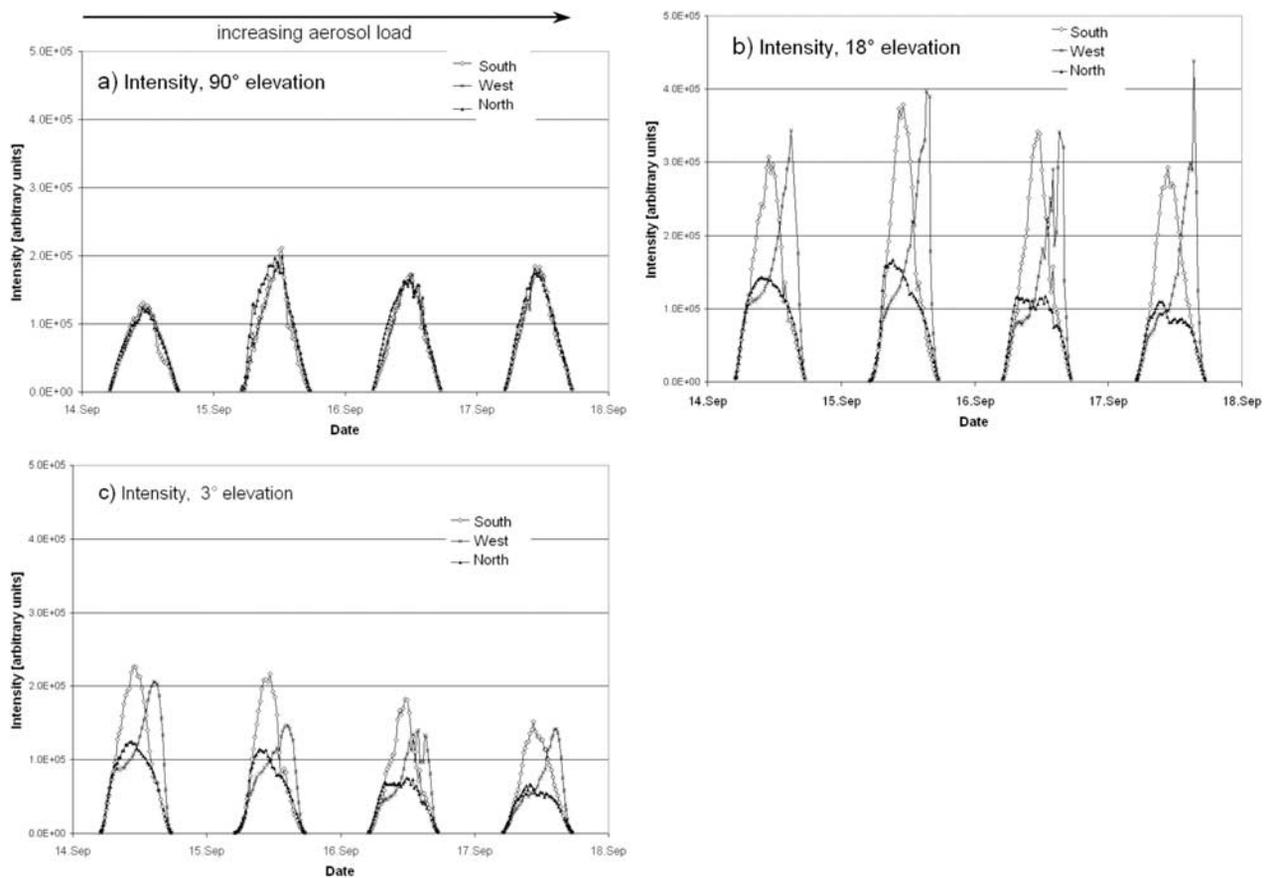
Figure 10. (a) Measured broadband intensity (average for 335–464 nm) for the different telescopes (north, south, west) at 90° elevation for September 14 to 17 in relative units. The observations during the morning of September 15 were affected by clouds and should not taken into account for the detailed interpretation of the time series. (b) Measured broadband intensity for 18° telescope elevation and different azimuth angles (north, south, west). The intensities of the telescopes at different azimuth angles are not directly comparable, because of different transmissions of the respective entrance optics. In order to allow a useful comparison, the intensities of the different telescopes were normalized according to the respective measurements in zenith direction. (c) Measured broadband intensity for 3° telescope elevation and different azimuth angles (north, south, west).

into account multiple scattering, and full sphericity [*von Friedeburg*, 2003; *Hönninger et al.*, 2004]. The aim of these numerical simulations was not to exactly match the values of our MAX-DOAS observations. This will be the subject of a further detailed study. Our intention here was to test each of the findings described in section 4 in principle. Our simulations are thus restricted to a small set of four aerosol profiles, which differ in vertical extent and optical depth (see Table 4). In addition, also simulations for a hypothetical pure Rayleigh atmosphere were performed.

[56] It should be also noted that the current version of our radiative transfer model does not include a full representation of polarization. This might introduce small errors, especially for situations in which the viewing geometry will prefer scattering of one polarization direction (like, e.g., during sunrise or sunset). However, to our knowledge this influence is insignificant with respect to the basic conclusions of our study.

[57] The results of our simulations are the O$_4$ absorption (expressed as AMF), the intensity, and the Ring effect.

Usually the modeled atmospheric trace gas absorptions are expressed as air mass factors (AMF), which represent the ratio between the slant column density (SCD) and the vertical column density (VCD) [*Noxon et al.*, 1979; *Solomon et al.*, 1987; *Marquard et al.*, 2000]. With the knowledge of the O$_4$ VCD at the measuring site, these AMFs can also be converted into the O$_4$ SCDs (and vice versa), which is one convenient way to compare measurements and model results also in an absolute way. Assuming a ground pressure and temperature of 1000 hPa and 293 K, respectively, we calculated an O$_4$ VCD of $1.19 \cdot 10^{43}$ molec^2/cm^5. This value takes into account the surface elevation of the measuring site of about 140 m. We used this O$_4$ VCD of $1.19 \cdot 10^{43}$ molec^2/cm^5 for the comparison of the measured O$_4$ SCD with the modeled O$_4$ AMF. For that purpose a second y-axis is added at the left-hand side of Figures 5, 6, and 8. Please note that the AMF axes are shifted according to the O$_4$ absorption of the Fraunhofer reference spectrum which is about 1.8 (expressed as AMF for a zenith viewing telescope at SZA of 40°, see Figure 12).
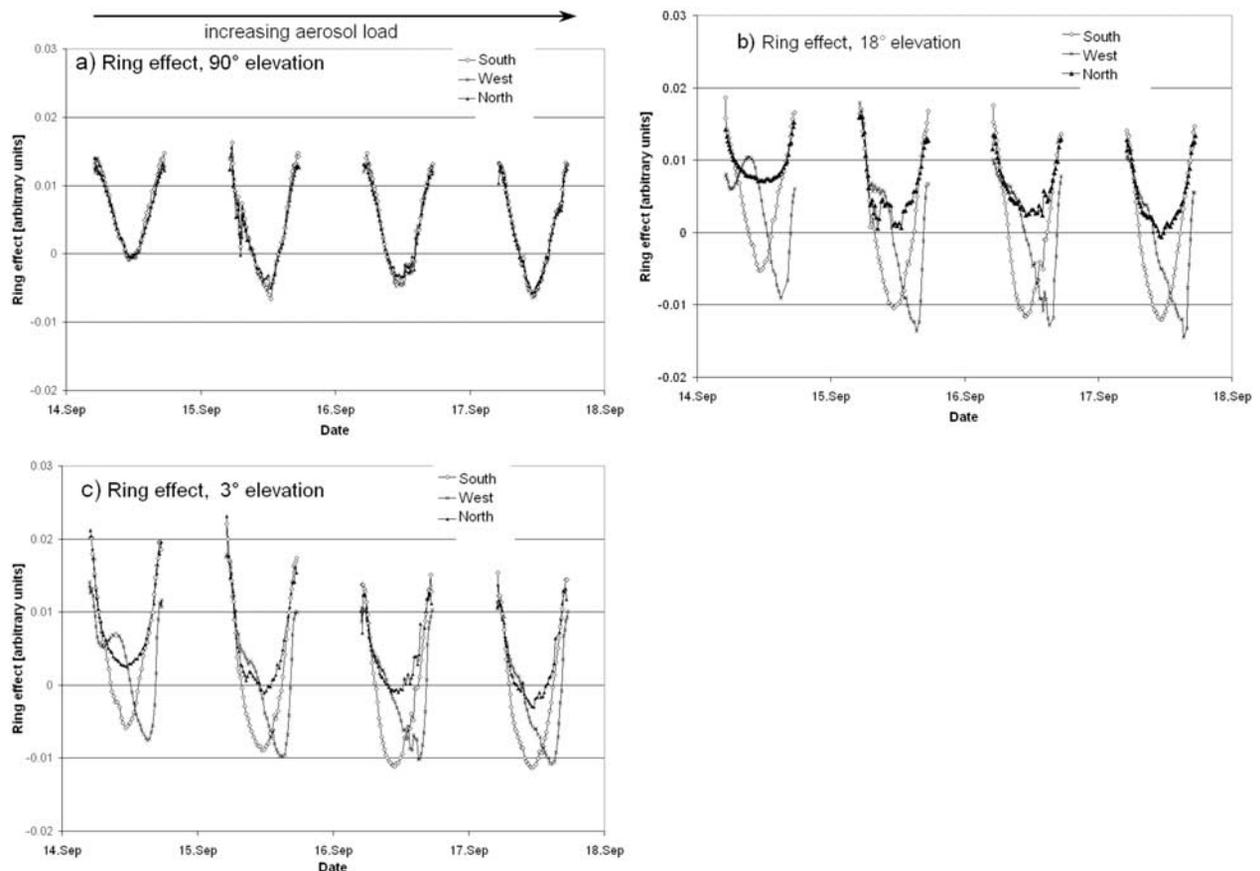
Figure 11. (a) Ring effect for observations of the different telescopes at 90° elevation for September 14 to 17 in relative units. The displayed values represent the difference of the Ring effect between the actual measurement and the reference spectrum. The observations during the morning of September 15 were affected by clouds and should not be taken into account for the detailed interpretation of the time series. (b) Ring effect for 18° elevation and different azimuth angles (north, south, west). (c) Ring effect for 3° elevation and different azimuth angles (north, south, west).

The respective O$_4$ SCD is about $2.2 \cdot 10^{43}$ molec^2/cm^5. The shift of the AMF axis allows the direct comparison between the measured DSCDs and the modeled (absolute) AMFs.

5.1. Reduction of the Direct Light Path Along the Line of Sight

[58] In Figure 12 the modeled O$_4$ AMFs for different elevation angles and different aerosol profiles are shown as a function of SZA. The azimuth angle was set to 0. While additional aerosol scattering has only a small influence on the AMFs for zenith direction, the AMFs for the low elevation angles are strongly affected by the different aerosol loads. In general, the finding that the AMFs become smaller for increasing aerosol extinction is clearly confirmed. In particular it is shown that especially the telescopes at low elevation are very sensitive to aerosol scattering near the surface. One additional interesting finding is that the telescopes at low elevation angles are also very sensitive to the aerosol height profile. In particular for the two aerosol profiles with the same total optical depth (0.05) from either 0 to 2 km or 0 to 1 km the respective O$_4$ AMFs are significantly different. We conclude that the general dependencies of our model results are in excellent

agreement with the MAX-DOAS O$_4$ measurements and the discussion given in sections 3 and 4.

[59] For the absolute values we also find a good agreement for most cases. For example, the high O$_4$ SCDs for the 3° telescope on the morning of September 14 are well described by the respective AMFs for a pure Rayleigh atmosphere (modeled AMF: 7.3 compared to the measurement of 7.4) indicating that the atmosphere was indeed very clean after the rainy days. In the course of this day the observed O$_4$ SCDs decrease, indicating that significant amounts of aerosols are again present. On the morning of the last day the O$_4$ SCD expressed as AMFs for all low elevation telescopes are only 4.6 which is slightly above the modeled values (AMF = 4.5) for the aerosol profile with an optical depth of 0.5. The noon values of this day of 2.2 are also in good agreement with the AMFs of 2.6 for this profile.

[60] We also found some observations which cannot be well described by the limited set of AMFs calculated within this study (e.g., the observed O$_4$ SCDs for the 18° telescope on September 14 seem to be higher than all modeled AMFs). This is probably caused by the relative azimuth angles of the measurement with respect to the Sun, which
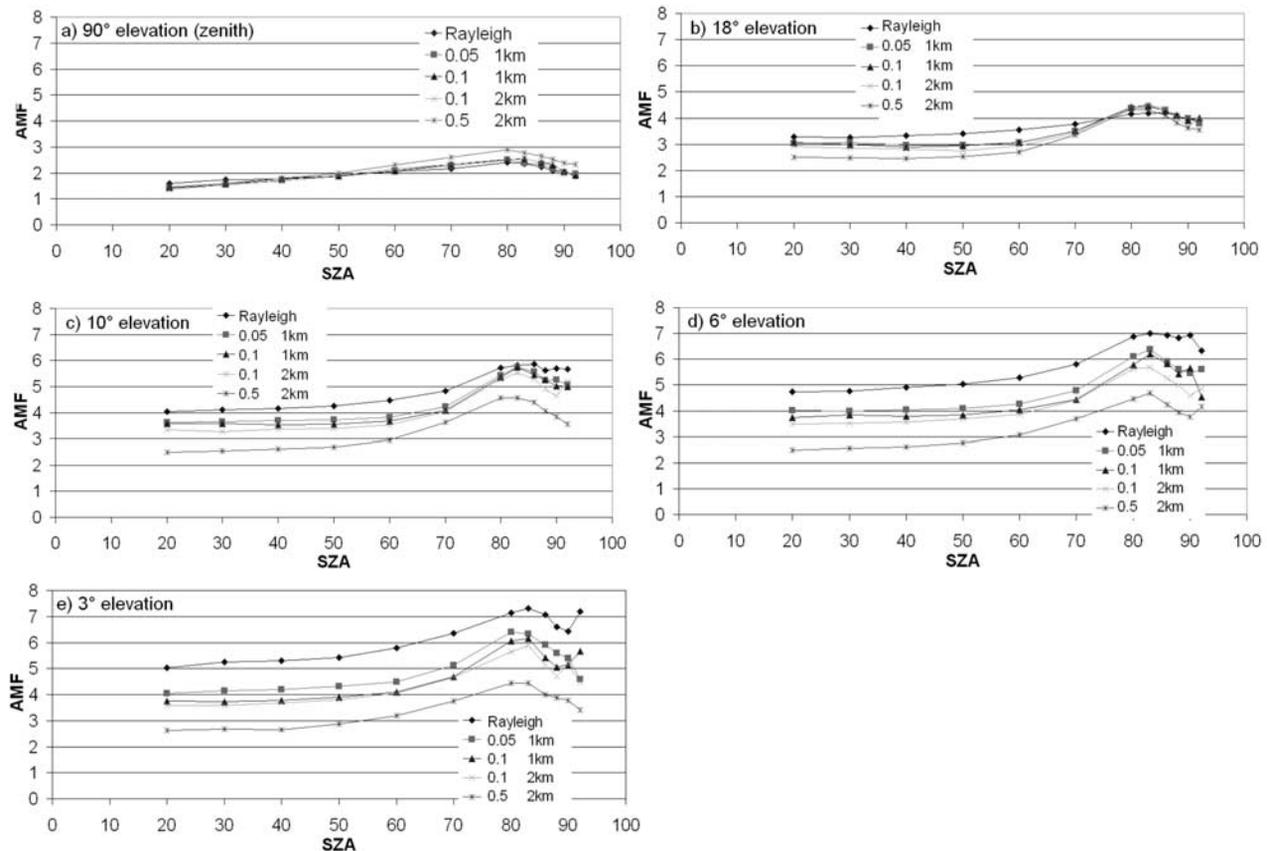
Figure 12. (a) O$_4$ AMF calculated with the Monte Carlo model 'TRACY' [*von Friedeburg*, 2003] for 90° telescope elevation and different aerosol scenarios. The first number in the legend indicates the aerosol extinction per km; the second number indicates the upper boundary of the aerosol layer (see Table 4). (b) O$_4$ AMF for 18° telescope elevation. (c) O$_4$ AMF for 10° telescope elevation. (d) O$_4$ AMF for 6° telescope elevation. (e) O$_4$ AMF for 3° telescope elevation. See color version of this figure at back of this issue.

are around 90° compared to 0° for the modeling results. However, as stated before, in this study our main aim is to illustrate the general dependencies of the MAX-DOAS O$_4$ observations and not to exactly match our MAX-DOAS observations.

5.2. Influence on the Penetration Depth of the Incident Sunlight

[61] In Figure 12 it can also be seen that the amplitude of the AMF variation during the day is influenced by the aerosol profile. For the zenith viewing telescopes it is slightly increased if the aerosol scattering is enhanced: from about 0.8 for a pure Rayleigh atmosphere to about 1.1 for the aerosol layer with an optical depth of 0.5 (see Table 4), in excellent agreement with the MAX-DOAS observations. For the low elevation telescopes, the modeled values seem to underestimate the observed values. This might, however, partly be because the radiative transport modeling was performed for an azimuth angle of 0 (see also section 5.5).

5.3. Effects of Multiple Scattering

[62] We investigated the effects of multiple scattering inside vertically extended clouds. O$_4$ AMFs for MAX-DOAS observations were calculated for three different cases: (1) a cloud with a total optical depth of 5 and a vertical extension from 0.1 to 5 km, (2) a cloud with a total

optical depth of 20 and a vertical extension from 0.1 to 2 km, and (3) a cloud with a total optical depth of 50 and a vertical extension from 0.1 to 5 km. The results are summarized in Figure 13. We find that the O$_4$ AMF is strongly enhanced for optically thick clouds and depends only slightly on elevation angle. The number of scattering events can become very large: for the cloud with an optical depth of 50, it is almost 1000. The enhanced O$_4$ absorptions of September 9 (see section 4.3) are in reasonable agreement with the O$_4$ AMFs for the cloud with an optical depth of 20.

5.4. Influence of Aerosol Absorption

[63] We investigated how strongly the absorbing properties of aerosols affect the MAX-DOAS O$_4$ observations. It turned out that in contrast to the total intensity of the observed light, the O$_4$ absorption is only weakly affected (Figure 14). This finding can be explained by the fact that even for strong absorbing aerosols, the average photon path lengths are still high; it indicates one potential specific advantage of O$_4$ MAX-DOAS observations for the determination of aerosol properties.

5.5. Influence of the Scattering Phase Function

[64] We modeled MAX-DOAS O$_4$ AMFs, the intensity, and the Ring effect (Figure 15) as a function of the azimuth angle (between the telescopes and the Sun). As expected,
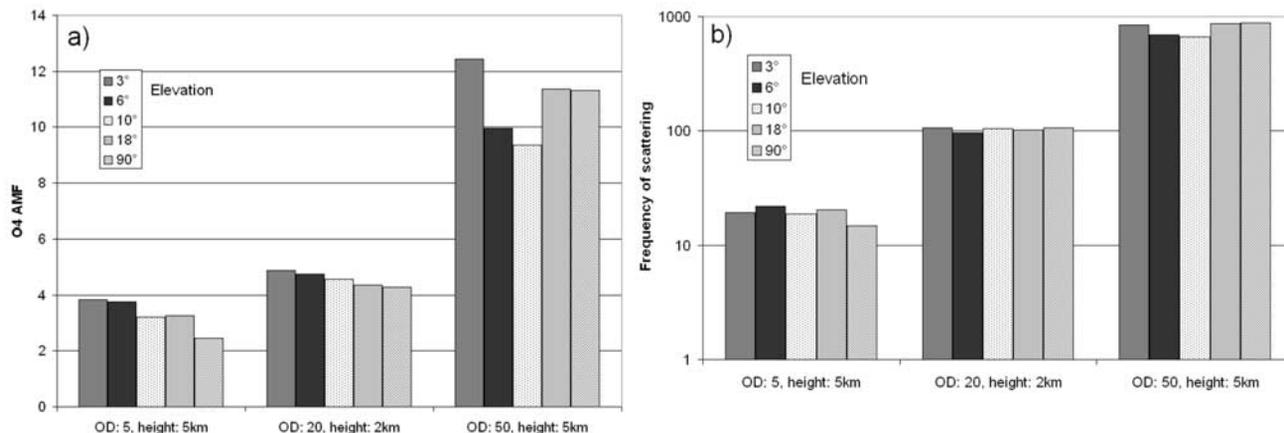
Figure 13. (a) O$_4$ AMFs for clouds with different optical depths and different vertical extensions. The assumed clouds are located close to the ground (cloud base height 100 m) and the O$_4$ AMF only slightly depends on the elevation angle. (b) Number of scattering events for clouds with different optical depths and different vertical extensions.

the O$_4$ AMFs are smallest for an azimuth angle of 0 (see section 4.5). For this angle, single scattering on aerosols has a larger relative contribution to the total intensity compared to other azimuth angles. Accordingly, for an azimuth angle of 0° the intensity is highest and the Ring effect is smallest because of the preferred forward scattering of aerosols. These findings are in excellent agreement with our observations (section 4.5).

[65] It should be noted here that our radiative transfer model so far does not include a realistic module for the detailed simulation of the Ring effect. In this study, we approximated the relative strength of the Ring effect from the relative contribution of photons having undergone molecular scattering to the total number of scattering events.

5.6. Sensitivity of the Method

[66] MAX-DOAS observations are based on differential absorption spectroscopy and thus do not require an absolute radiometric calibration. Therefore the method is sensitive even to very weak aerosol optical depths. In order to assess the detection limit of MAX-DOAS O$_4$ aerosol observations, we simulated O$_4$ absorptions for different viewing geometries and wavelengths; Figure 16 shows results for 360 and 630 nm.

[67] Even for very small aerosol optical depths, the O$_4$ absorptions are significantly reduced. For example, an aerosol extinction of 0.5% reduces the O$_4$ absorption at 630 nm for 3° elevation by about 12%. As to be expected, the reduction is stronger at longer wavelengths because there Rayleigh scattering is less important. In the red spectral range, MAX-DOAS O$_4$ observations are also more sensitive because the O$_4$ absorption cross section is much larger than in the UV spectral range. Assuming typical measurement errors for the O$_4$ absorption band at 630 nm, we conclude that aerosol optical depths >0.001 should be clearly detectable by MAX-DOAS O$_4$ observations. This estimate is based on the assumption that information on
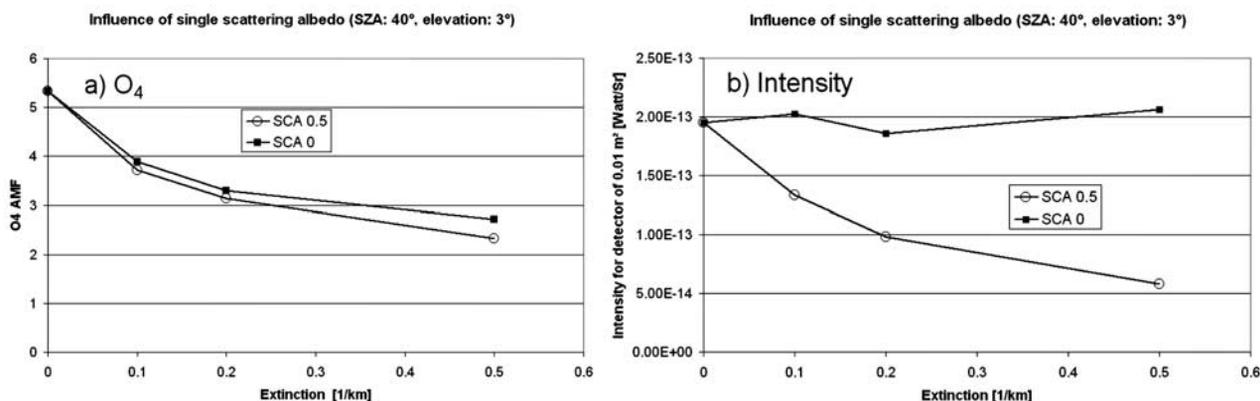

Figure 14. (a) Dependence of the MAX-DOAS O$_4$ AMF (for 3° elevation) for different aerosol optical depths and different values of the single scattering albedo. The MAX-DOAS O$_4$ absorption depends only weakly on the absorbing properties of aerosols. (b) Dependence of the observed intensity (for 3° elevation) for different aerosol optical depths and different values of the single scattering albedo. It strongly depends on the absorbing properties of aerosols.
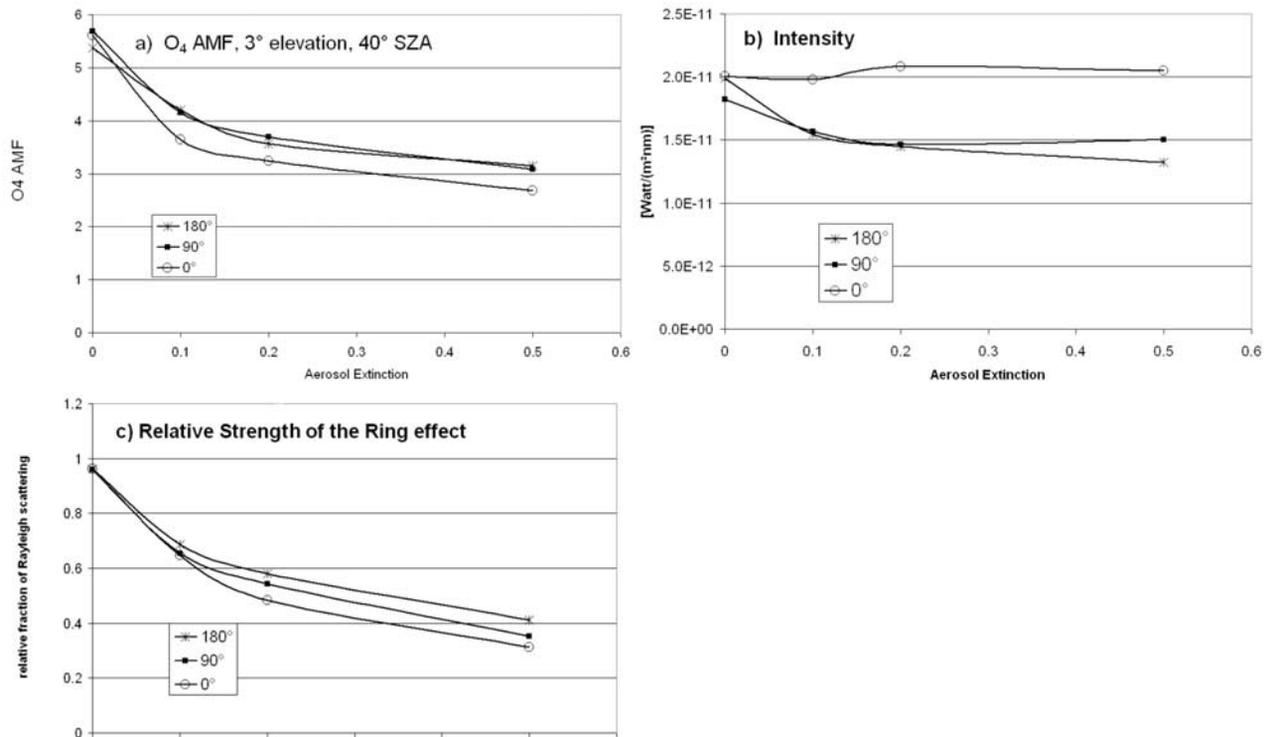
Figure 15. (a) O$_4$ AMF calculated for different MAX-DOAS elevation and azimuth angles. In agreement with MAX-DOAS observations the smallest O$_4$ absorptions are found for an azimuth angle of zero. This indicates the strong forward preference of aerosol scattering. (b) Intensity calculated for different MAX-DOAS elevation and azimuth angles. In agreement with MAX-DOAS observations the highest intensity is found for an azimuth angle of zero. This also indicates the strong forward preference of aerosol scattering. (c) Ring effect calculated for different MAX-DOAS elevation and azimuth angles. In agreement with MAX-DOAS obervations the strongest Ring effect is found for an azimuth angle of zero. This also indicates the strong forward preference of aerosol scattering.

surface pressure is available for an accurate determination of the atmospheric O$_4$ VCD for the respective observations.

6. Conclusions

[68] We have shown that MAX-DOAS O$_4$ observations are well suited as a potential new method for the determination of atmospheric aerosol properties (not dried). Compared to established methods like Sun radiometers and LIDAR measurements, the proposed method has two major advantages: Since they analyze the differential O$_4$ absorption structures, they do not require an absolute radiometric calibration or application of Langley-plot techniques. Thus they are, in particular, insensitive to instrument degradation. In addition, since the atmospheric O$_4$ profile depends strongly on altitude, MAX-DOAS O$_4$ observations are
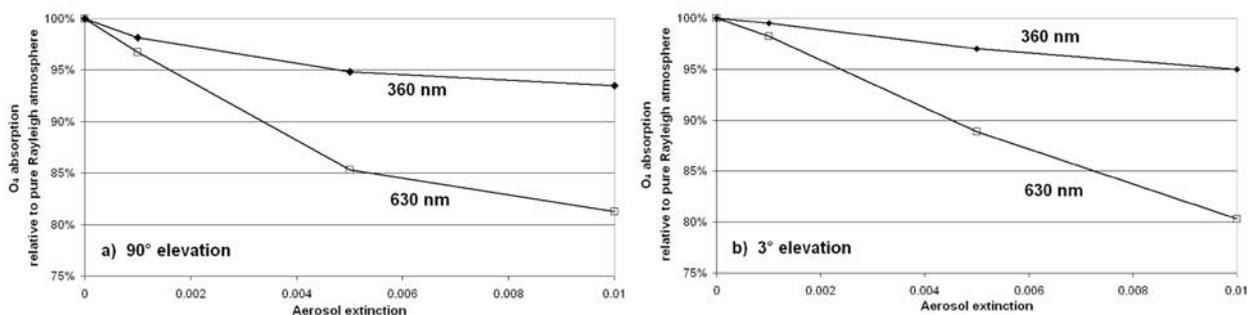

Figure 16. (a) O$_4$ absorptions modeled for different an elevation angle of 90° and different wavelengths. The O$_4$ absorptions are normalized with respect to those for a pure Rayleigh atmosphere. Especially at longer wavelengths aerosol optical depths below 0.001 could be detected by MAX-DOAS O$_4$ observations. (b) O$_4$ absorptions modeled for different an elevation angle of 3° and different wavelengths. The O$_4$ absorptions are normalized with respect to those for a pure Rayleigh atmosphere.

Table 5. Wavelengths and Transition Assignments of the O$_4$ Absorption Bands[a]

Wavelength, nm	Upper State of Transition (From $^3\sum_g^- + {}^3\sum_g^-$ Ground State)
343.4	$^1\sum_g^+ + {}^1\sum_g^+$ ($\nu = 2$)
360.5	$^1\sum_g^+ + {}^1\sum_g^+$ ($\nu = 1$)
380.2	$^1\sum_g^+ + {}^1\sum_g^+$ ($\nu = 0$)
446.7	$^1\sum_g^+ + {}^1\Delta_g$ ($\nu = 1$)
477.3	$^1\sum_g^+ + {}^1\Delta_g$ ($\nu = 0$)
532.2	$^1\Delta_g + {}^1\Delta_g$ ($\nu = 2$)
577.2	$^1\Delta_g + {}^1\Delta_g$ ($\nu = 1$)
630.0	$^1\Delta_g + {}^1\Delta_g$ ($\nu = 0$)

[a]For atmospheric observations, O$_4$ absorption bands throughout the UV-vis spectral range can be investigated [see, e.g., *Greenblatt et al.*, 1990; *Wagner et al.*, 2002].

sensitive to the atmospheric light path distribution. Therefore they can especially yield information on the atmospheric aerosol profile. The set of the elevation angles (and also azimuth angles and selected absorption bands) can be optimized with respect to the specific atmospheric conditions and measurement objectives. Current versions of MAX-DOAS instruments are lightweight and can be operated automatically. Thus they are especially well suited for remote observations.

[69] Using MAX-DOAS observations during clear days, we investigated several aspects of the aerosol influence in detail. These findings were also confirmed by atmospheric radiative transfer modeling and can be summarized as follows:

[70] 1. MAX-DOAS O$_4$ observations are very sensitive to the aerosol extinction close to the ground.

[71] 2. They are sensitive to the penetration depth of the incident solar radiation. Thus they can yield information on the altitude of the aerosol layer.

[72] 3. From the comparison of the observed O$_4$ absorption and the measured intensity, information on the absorbing properties of the aerosols might be derived.

[73] 4. Measurements at different wavelengths can characterize the wavelength dependence of the aerosol scattering, and thus yield information on the size distribution.

[74] 5. Not only the O$_4$ absorption can be analyzed but also the magnitude of the Ring effect and the (relative) intensity can be investigated. These quantities can also be used for the determination of aerosol properties. In addition, also the absorption of the O$_2$ molecule should be investigated.

[75] 6. Owing to the differences in the polarizing properties of aerosols and Rayleigh scattering, additional information on aerosol properties might be derived from observations of light with different polarization orientation.

[76] 7. From MAX-DOAS O$_4$ observations at different azimuth angles, information on the scattering phase function can be derived.

[77] 8. MAX-DOAS O$_4$ absorptions are very sensitive: aerosol optical depths below 0.001 can probably be detected.

[78] It should be noted that like observations by Sun photometers and LIDAR instruments, also MAX-DOAS observations are affected by clouds. Nevertheless, especially compared to Sun photometers, these restrictions can be expected to be much less important for two reasons. First,

even for observations under a cloud cover, information on surface near aerosol layers can still be derived from the low elevation telescopes. This is because, for these telescopes, the light path through the surface near high O$_4$ concentrations is still almost exclusively determined by the surface near aerosols. Second, since no Langley plot techniques are needed, already very short clear periods between clouds are sufficient for the application of our new method.

[79] In this study, our main aim was to present a new method and outline its potentials. It is clear that the full potential of the method must be investigated in additional detailed future studies. In particular the wavelength and polarization dependence of the atmospheric O$_4$ absorption should be explored in more detail. Throughout the UV-vis spectral range several O$_4$ absorption bands can be observed by MAX-DOAS instruments (see Table 5). Since the probability of Rayleigh scattering depends strongly on wavelength, the effect of additional aerosol scattering differs significantly for these absorption bands [see also *Wagner et al.*, 2002].

[80] We hope that the suitability of MAX-DOAS O$_4$ observations can be tested in combined field campaigns with simultaneous aerosol observations by other methods, in particular Sun photometers and LIDAR observations. We are confident that from a combination of the results with these methods, synergistic use can be made for the determination of atmospheric aerosol properties. In particular, total aerosol optical depth measurements by Sun photometers as well as aerosol profiles by LIDAR instruments can provide very valuable information for the interpretation and validation of MAX-DOAS O$_4$ measurements.

[81] Future work will, in particular, include more extensive radiative transport modeling to describe in more detail the response of the observations to a comprehensive set of aerosol scenarios. As a next step, inversion schemes will be developed for the systematic exploitation of the information content of MAX-DOAS O$_4$ observations on atmospheric aerosols.

References

Aliwell, S. R., et al. (2002), Analysis for BrO in zenith-sky spectra: An intercomparison exercise for analysis improvement, *J. Geophys. Res.*, 107(D14), 4199, doi:10.1029/2001JD000329.

Ansmann, A., M. Riebesell, and C. Weitcamp (1990), Measurement of atmospheric aerosol extinction profiles with a Raman lidar, *Opt. Lett.*, 15, 746–748.

Ansmann, A., U. Wandinger, M. Riebesell, C. Weitcamp, and W. Michaelis (1992), Independent measurement of extinction and backscatter profiles in cirrus clouds by using a combined Raman elastic-backscatter lidar, *Optics*, 31, 7113–7131.

Barrett, E. W., and O. Ben-Dov (1967), Application of the lidar to air pollution measurements, *J. Appl. Meteorol.*, 6, 500.

Bobrowski, N., G. Hönninger, B. Galle, and U. Platt (2003), Detection of bromine monoxide in a volcanic plume, *Nature*, 423, 273–276.

Bogumil, K., et al. (2003), Measurements of molecular absorption spectra with the SCIAMACHY pre-flight model: Instrument characterization and reference data for atmospheric remote-sensing in the 230–2380 nm region, *J. Photochem. Photobiol. A*, 157, 167–184.

Box, M. A., and A. Deepak (1979), Retrieval of aerosol size distribution by inversion of solar aureole data in the presence of multiple scattering, *Appl. Opt.*, 18, 1376–1382.

Bussemer, M. (1993), Der Ring-Effekt: Ursachen und Einfluß auf die Messung stratosphärischer Spurenstoffe, diploma thesis, Univ. of Heidelberg, Heidelberg, Germany.

Chance, K. V., and R. J. D. Spurr (1997), Ring effect studies: Rayleigh scattering, including molecular parameters for rotational Raman scattering, and the Fraunhofer spectrum, *Appl. Opt.*, *36*(21), 5224–5230.

Charlson, R. J., S. E. Schwartz, J. M. Hales, R. D. Cess, J. A. Coakley Jr., J. E. Hansen, and D. J. Hofmann (1992), Climate forcing by anthropogenic aerosol, *Science*, *255*, 423–430.

Collis, R. T. H. (1966), Lidar: A new atmospheric probe, *Q. J. R. Meteorol. Soc.*, *92*, 220–230.

Devaux, C., A. Vermeulen, J. L. Deuzé, P. Dubuisson, M. Herman, R. Santer, and M. Verbrugghe (1998), Retrieval of aerosol single-scattering albedo from ground-based measurements: Application to observational data, *J. Geophys. Res.*, *103*, 8753–8761.

Erle, F., K. Pfeilsticker, and U. Platt (1995), On the influence of tropospheric clouds on zenith-scattered-light measurements of stratospheric species, *Geophys. Res. Lett.*, *22*, 2725–2728.

Feingold, G., W. R. Cotton, S. M. Kreidenweis, and J. T. Davis (1999), Impact of giant cloud condensation nuclei on drizzle formation in marine stratocumulus: Implications for cloud radiative properties, *J. Atmos. Sci.*, *56*, 4100–4117.

Fernald, F. G. (1984), Analysis of atmospheric lidar observations: Some comments, *Appl. Opt.*, *23*, 652–653.

Fernald, F. G., B. M. Herman, and J. A. Reagan (1972), Determination of aerosol height distribution by lidar, *J. Appl. Meteorol.*, *11*, 482–489.

Ferrare, R. A., S. H. Melfi, D. N. Whiteman, K. D. Evans, and R. Leifer (1998), Raman lidar measurements of aerosol extinction and backscattering: 1. Methods and comparisons, *J. Geophys. Res.*, *103*, 19,663–19,672.

Gomer, T., T. Brauers, F. Heintz, J. Stutz, and U. Platt (1993), MFC user manual, version 1.98, Inst. für Umweltphys., Univ. of Heidelberg, Heidelberg, Germany.

Grainger, J. F., and J. Ring (1962), Anomalous Fraunhofer line profiles, *Nature*, *193*, 762.

Greenblatt, G. D., J. J. Orlando, J. B. Burkholder, and A. R. Ravishankara (1990), Absorption measurements of oxygen between 330 and 1140 nm, *J. Geophys. Res.*, *95*, 18,577–18,582.

Hamilton, P. M. (1969), Lidar measurements of backscatter and attenuation of atmospheric aerosols, *Atmos. Environ.*, *3*, 221–223.

Hansen, J., M. Sato, and R. Ruedy (1997), Radiative forcing and climate response, *J. Geophys. Res.*, *102*, 6831–6864.

Holben, B. N., et al. (1998), AERONET—A federated instrument network and data archive for aerosol characterization, *Remote Sens. Environ.*, *66*(1), 1–16.

Hönninger, G., and U. Platt (2002), The role of BrO and its vertical distribution during surface ozone depletion at Alert, *Atmos. Environ.*, *36*, 2481–2489.

Hönninger, G., C. von Friedeburg, and U. Platt (2004), Multi Axis Differential Optical Absorption Spectroscopy (MAX-DOAS), *Atmos. Chem. Phys.*, *4*, 231–254.

Houghton, J. T., , Y. Ding, D. J. Griggs, M. Noguer, P. J. van der Linden, and D. Xiaosu (Eds.) (2001), *Climate Change 2001: The Scientific Basis—Contribution of Working Group I to the Third Assessment Report of the Intergovernmental Panel on Climate Change (IPCC)*, 944 pp., Cambridge Univ. Press, New York.

Hughes, H. G., and M. R. Paulson (1988), Double-ended lidar technique for aerosol studies, *Appl. Opt.*, *27*, 2273–2278.

Kattawar, G. W., A. T. Young, and T. J. Humphreys (1981), Inelastic scattering in planetary atmospheres. I. The Ring Effect, without aerosols, *Astrophys. J.*, *243*, 1049–1057.

Kaufman, Y. J., A. Gitelson, A. Karnieli, E. Ganor, R. S. Fraser, T. Nakajima, S. Mattoo, and B. N. Holben (1994), Size distribution and scattering phase function of aerosol particles retrieved from sky brightness measurements, *J. Geophys. Res.*, *99*, 10,341–10,356.

Kaufman, Y. J., D. Tanré, and O. Boucher (2002), A satellite view of aerosols in the climate system, *Rev. Nature*, *419*, 215–223.

Kaufman, Y. J., D. Tanré, J.-F. Léon, and J. Pelon (2003), Retrievals of profiles of fine and coarse aerosols using lidar and radiometric space measurements, *IEEE Trans. Geosci. Remote Sens.*, *41*(8), 1743–1754.

King, M. D., D. M. Byrne, B. N. Herman, and J. A. Reagan (1978), Aerosol size distributions obtained by inversion of spectral optical depth measurements, *J. Atmos. Sci.*, *35*, 2153–2167.

Klett, J. D. (1981), Stable analytical inversion solution for processing lidar returns, *Appl. Opt.*, *20*, 211–220.

Kunz, G. J. (1987), Bipath method as a way to measure the spatial backscatter and extinction coefficients with lidar, *Appl. Opt.*, *26*, 794–795.

Kurucz, R. L., I. Furenlid, J. Brault, and L. Testerman (1984), Solar flux atlas from 296 nm to 1300 nm, *Natl. Sol. Obs. Atlas*, *1*.

Leser, H., G. Hönninger, and U. Platt (2003), MAX-DOAS measurements of BrO and NO$_2$ in the marine boundary ayer, *Geophys. Res. Lett.*, *30*(10), 1537, doi:10.1029/2002GL015811.

Marquard, L. C., T. Wagner, and U. Platt (2000), Improved air mass factor concepts for scattered radiation differential optical absorption spectroscopy of atmospheric species, *J. Geophys. Res.*, *105*, 1315–1327.

Meller, R., and G. K. Moortgat (2000), Temperature dependence of the absorption cross sections of formaldehyde between 223 and 323 K in the wavelength range 225–375 nm, *J. Geophys. Res.*, *105*, 7089–7101.

Nakajima, T., M. Tanaka, and T. Yamauchi (1983), Retrieval of the optical properties of aerosols from aureole and extinction data, *Appl. Opt.*, *22*, 2951–2959.

Nakajima, T., G. Tonna, R. Rao, P. Boi, Y. Kaufman, and B. Holben (1996), Use of sky brightness measurements from ground for remote sensing of particulate dispersion, *Appl. Opt.*, *35*, 2672–2686.

Noxon, J. F., E. C. Whipple, and R. S. Hyde (1979), Stratospheric NO$_2$: 1. Observational method and behavior at midlatitudes, *J. Geophys. Res.*, *84*, 5047–5076.

O'Neill, N. T., and J. R. Miller (1984), Combined solar aureole and solar beam extinction measurements. 2. Studies of the inferred aerosol size distribution, *Appl. Opt.*, *23*, 3697–3704.

Perliski, L. M., and S. Solomon (1993), On the evaluation of air mass factors for atmospheric near-ultraviolet and visible absorption spectroscopy, *J. Geophys. Res.*, *98*, 10,363–10,374.

Pfeilsticker, K. (1999), First geometrical path length distribution probability density function derivation of the skylight from spectroscopic highly resolved oxygen A-band observations: 2. Derivation of the Lévy-index for the skylight transmitted by midlatitude clouds, *J. Geophys. Res.*, *104*, 4104–4116.

Pfeilsticker, K., F. Erle, O. Funk, H. Veitel, and U. Platt (1998), First geometrical path lengths probability density function derivation of the skylight from spectroscopically highly resolving oxygen A-band observations: 1. Measurement technique, atmospheric observations, and model calculations, *J. Geophys. Res.*, *103*, 11,483–11,504.

Pfeilsticker, K., et al. (1999), Intercomparison of the measured influence of tropospheric clouds on UV-visible absorptions detected during the NDSC intercomparison campaign at OHP in June 1996, *Geophys. Res. Lett.*, *26*, 1169–1172.

Platt, U. (1994), Differential optical absorption spectroscopy (DOAS), in *Air Monitoring by Spectroscopic Techniques, Chem. Anal. Ser.*, vol. 127, edited by M. W. Sigrist, John Wiley, Hoboken, N. J.

Ramanathan, V., P. J. Crutzen, J. T. Kiehl, and D. Rosenfeld (2001), Atmosphere—Aerosols, climate, and the hydrological cycle, *Science*, *294*, 2119–2124.

Reagan, J. A., J. D. Spinhirne, D. M. Byrne, D. W. Thomson, R.G. DePena, and Y. Mamane (1977), Atmospheric particulate properties inferred from Lidar and solar radiometer observations compared with simultaneous in situ aircraft measurements: A case study, *J. Appl. Meteorol.*, *16*, 911–928.

Romanov, P., N. T. O'Neill, A. Royer, and B. McArthur (1999), Simultaneous retrieval of aerosol refractive index and particle size distribution from ground based measurements of direct and scattered radiation, *Appl. Opt.*, *38*, 7305–7320.

Rosenfeld, D. (2000), Suppression of rain and snow by urban and industrial air pollution, *Science*, *287*, 1793–1796.

Rosenfeld, D., R. Lahav, A. P. Khain, and M. Pinsky (2002), The role of seaspray in cleansing air pollution over ocean via cloud processes, *Science*, *297*, 1667–1670.

Sandford, M. C. W. (1967), Laser scatter measurements in the mesosphere and above, *J. Atmos. Terr. Phys.*, *29*, 1657–1662.

Shaw, G. E. (1979), Inversion of optical scattering and spectral extinction measurements to recover aerosol size spectra, *Appl. Opt.*, *18*, 988–993.

Solomon, S., A. L. Schmeltekopf, and R. W. Sanders (1987), On the interpretation of zenith sky absorption measurements, *J. Geophys. Res.*, *92*, 8311–8319.

Spinhirne, J. D., J. A. Reagan, and B. M. Herman (1980), Vertical distribution of aerosol extinction cross section and inference of aerosol imaginary index in the troposphere by lidar technique, *J. Appl. Meteorol.*, *19*, 426–438.

Stutz, J., and U. Platt (1996), Numerical analyses and estimation of the statistical error of differential optical absorption spectroscopy measurements with least square methods, *Appl. Opt.*, *35*, 6041–6053.

Tanré, D., C. Deuaux, M. Herman, and R. Santer (1988), Radiative properties of desert aerosols by optical ground-based measurements at solar wavelengths, *J. Geophys. Res.*, *93*, 14,223–14,231.

Tegen, I., and A. A. Lacis (1996), Modeling of particle size distribution and its influence on the radiative properties of mineral dust aerosol, *J. Geophys. Res.*, *101*, 19,237–19,244.

Twitty, J. T. (1975), The inversion of aureole measurements to derive aerosol size distributions, *J. Atmos. Sci.*, *32*, 584–591.

Twomey, S. A., M. Piepgrass, and T. L. Wolfe (1984), An assessment of the impact of pollution on the global albedo, *Tellus, Ser. B*, *36*, 356–366.

Vandaele, A. C., C. Hermans, P. C. Simon, M. Carleer, R. Colin, S. Fally, M.-F. Mérienne, A. Jenouvrier, and B. Coquart (1997), Measurements of the NO$_2$ absorption cross-section from 42000 cm-1 to 10000 cm-1 (238–1000 nm) at 220 K and 294 K, *J. Quant. Spectrosc. Radiat. Transfer*, *59*, 171–184.

van Roozendael, M., C. Fayt, P. Post, C. Hermans, and J.-C. Lambert (2003), Retrieval of BrO and NO$_2$ from UV-visible observations, in *Sounding the Troposphere From Space: A New Era for Atmospheric Chemistry*, edited by P. Borell et al., Springer-Verlag, New York.

Veitel, V., O. Funk, C. Kurz, U. Platt, and K. Pfeilsticker (1998), Geometrical path length probability density function of the skylight transmitted by mid-latitude cloudy skies; Some case studies, *Geophys. Res. Lett.*, *25*, 3355–3358.

Vermeulen, A., C. Devaux, and M. Herman (2000), Retrieval of the scattering and microphysical properties of aerosols from ground-based optical measurements including polarization. 1. Method, *Appl. Opt.*, *39*, 6207–6220.

Volz, F. E. (1959), Photometer mit Selen-Photoelement zur spektralen Messung der Sonnenstrahlung und zur Bestimmung der Wellenlangen-abhängigkeit der Dunsttrübung, *Arch. Meteorol. Geophys. Bioklimatol., Ser. B*, *l0*, 100–131.

von Friedeburg, C. (2003), Derivation of trace gas information combining differential optical absorption spectroscopy with radiative transfer modelling, Ph.D. thesis, Univ. of Heidelberg, Heidelberg, Germany.

von Friedeburg, C., I. Pundt, K.-U. Mettendorf, T. Wagner, and U. Platt (2004), Multi-AXis-(MAX) DOAS measurements of NO$_2$ during the BAB II Motorway Emission Campaign, *Atmos. Environ.*, in press.

Voss, K. J., E. J. Welton, P. K. Quinn, J. Johnson, A. M. Thompson, and H. R. Gordon (2001), Lidar measurements during Aerosols99, *J. Geophys. Res.*, *106*, 20,821–20,831.

Wagner, T., F. Erle, L. Marquard, C. Otten, K. Pfeilsticker, T. Senne, J. Stutz, and U. Platt (1998), Cloudy sky optical paths as derived from differential optical absorption spectroscopy observations, *J. Geophys. Res.*, *103*, 25,307–25,321.

Wagner, T., C. von Friedeburg, M. Wenig, C. Otten, and U. Platt (2002), UV/vis observations of atmospheric O$_4$ absorptions using direct moonlight and zenith scattered sunlight under clear and cloudy sky conditions, *J. Geophys. Res.*, *107*(D20), 4424, doi:10.1029/2001JD001026.

Wandinger, U., A. Ansmann, J. Reichardt, and T. Deshler (1995), Determination of stratospheric aerosol microphysical properties from independent extinction and backscattering measurements with a Raman lidar, *Appl. Opt.*, *34*, 8315–8329.

Wang, M., and H. R. Gordon (1993), Retrieval of the columnar aerosol phase function and single scattering albedo from sky radiance over the ocean: Simulations, *Appl. Opt.*, *32*, 4598–4609.

Wendisch, M., and W. von Hoyningen-Hüne (1994), Possibility of refractive index determination of atmospheric aerosol particles by ground-based solar extinction and scattering measurements, *Atmos. Environ.*, *28*, 785–792.

Wilmouth, D. M., T. F. Hanisco, N. M. Donahue, and J. G. Anderson (1999), Fourier transform ultraviolet spectroscopy of the A$^{2\Pi}_{3/2}$ ← X$^{2\Pi}_{3/2}$ transition of BrO, *J. Phys. Chem. A*, *103*, 8935–8945.

Wittrock, F., H. Oetjen, A. Richter, S. Fietkau, T. Medeke, A. Rozanov, and J. P. Burrows (2003), MAX-DOAS measurements of atmospheric trace gases in Ny-Ålesund, *Atmos. Chem. Phys. Discuss.*, *3*, 6109–6145.

Young, S. A., D. R. Cutten, M. J. L. Lynch, and J. E. Davies (1993), Lidar-derived variations in the backscatter-to-extinction ratio in southern hemispheric coastal maritime aerosols, *Atmos. Environ., Part A*, *27*, 1541–1551.

————————————

B. Dix, C. v. Friedeburg, U. Frieß, U. Platt, S. Sanghavi, R. Sinreich, and T. Wagner, Institut für Umweltphysik, University of Heidelberg, D-69120 Heidelberg, Germany. (thomas.wagner@iup.uni-heidelberg.de)
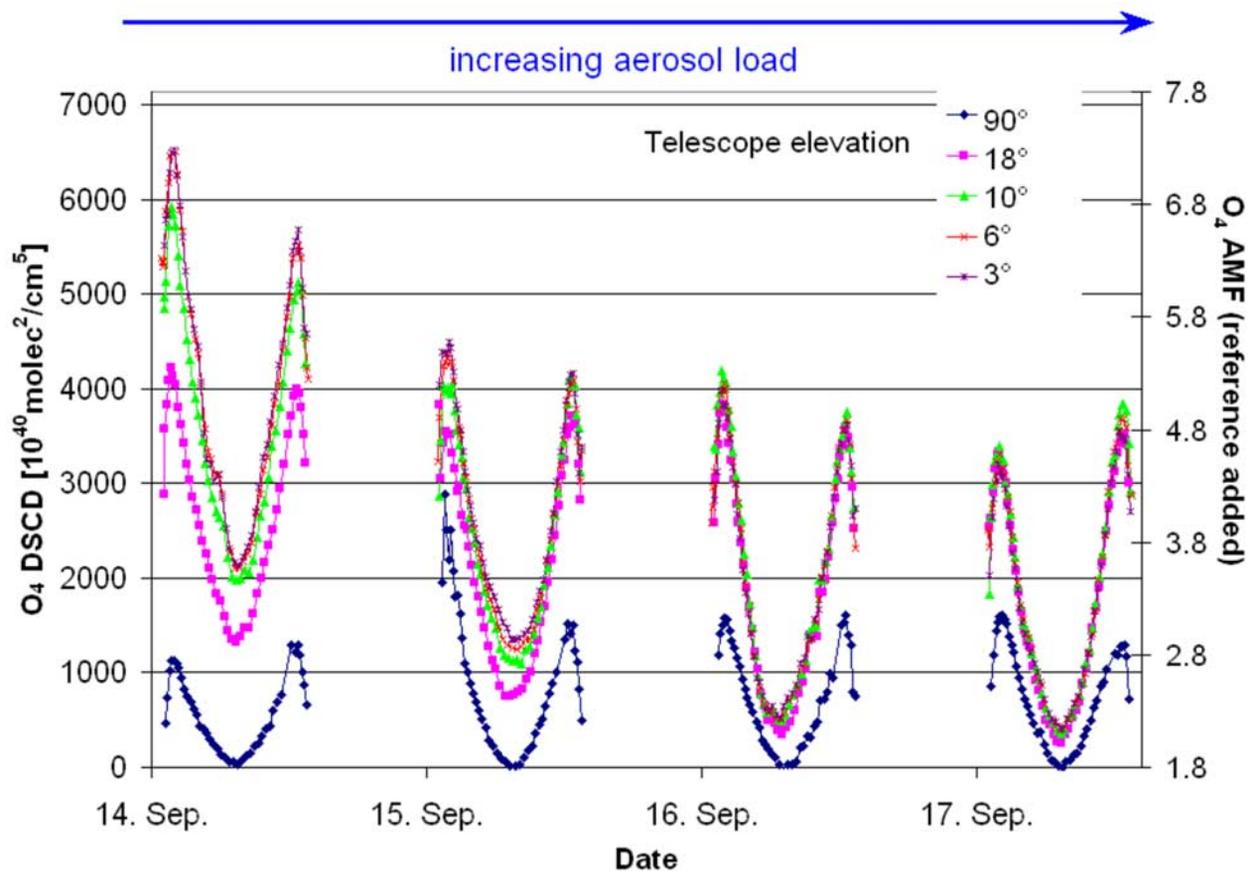
Figure 5. O$_4$ DSCDs measured for different elevation angles of the southern telescope during four mostly clear days (September 14–17, 2003) at Milan, Italy. Because of the changing Sun position during the day the relative azimuth angles of the telescopes with respect to the Sun are ~90° during sunrise, ~0° during noon, and ~−90° during sunset. The main effects are the general reduction of the observed O$_4$ absorption and the decreasing difference between the low elevation telescopes (3°, 6°, 10°, 18°). These effects can be related to the increased aerosol load during the selected period (see text). The zenith observations during the morning of September 15 were affected by sporadic clouds and should not be taken into account for the detailed interpretation of the time series. With the knowledge of the O$_4$ VCD and the O$_4$ absorption of the Fraunhofer reference spectrum, the measured O$_4$ DSCD can also be expressed as (absolute) air mass factor (AMF, see section 5). For the comparison of the measurements to radiative transfer models the respective AMF is also shown (right axis).
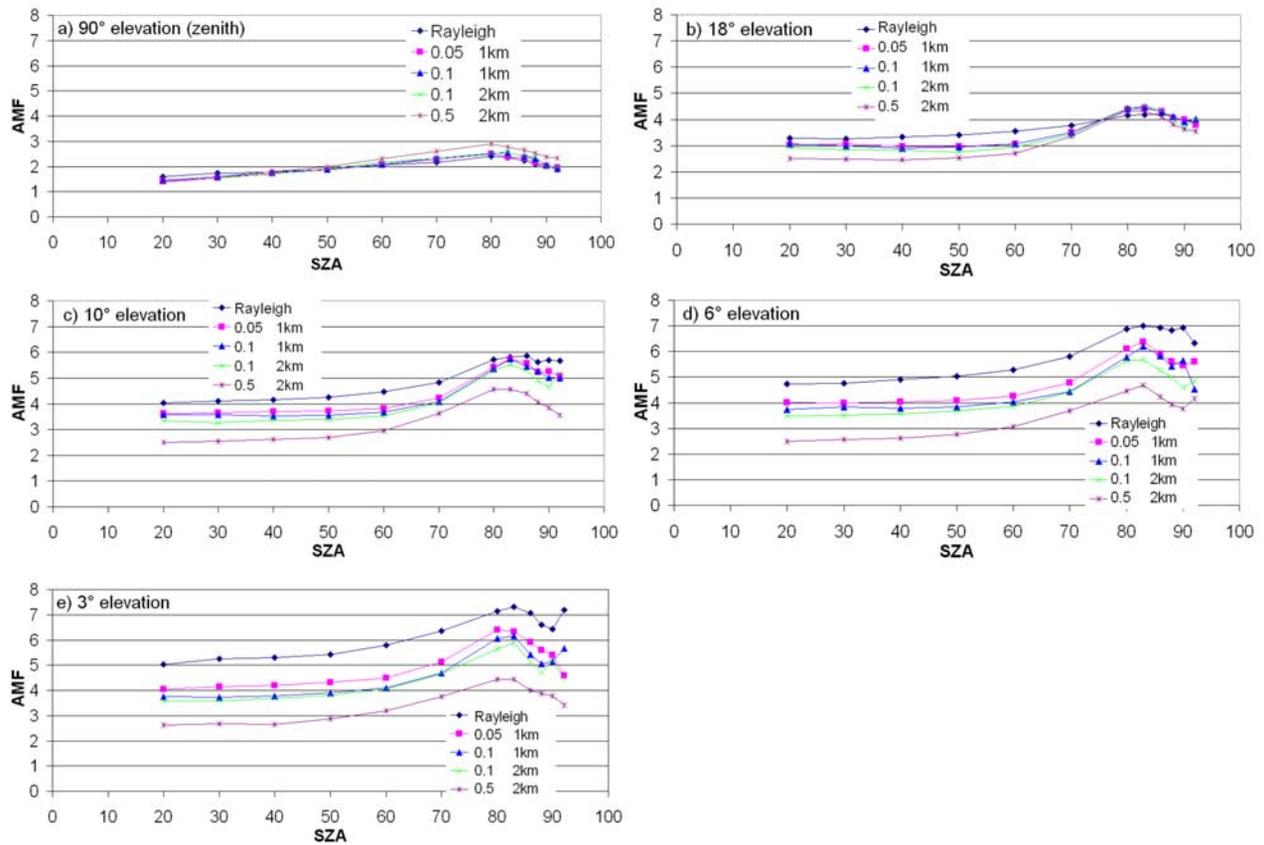
Figure 12. (a) O_4 AMF calculated with the Monte Carlo model 'TRACY' [*von Friedeburg*, 2003] for 90° telescope elevation and different aerosol scenarios. The first number in the legend indicates the aerosol extinction per km; the second number indicates the upper boundary of the aerosol layer (see Table 4). (b) O_4 AMF for 18° telescope elevation. (c) O_4 AMF for 10° telescope elevation. (d) O_4 AMF for 6° telescope elevation. (e) O_4 AMF for 3° telescope elevation.